CHAPTER – 4

ONE-DIMENSIONAL PHOTONIC CRYSTALS COMPOSED OF GRADED INDEX AND DISPERSIVE MATERIALS

4.1 Introduction

Photonic band gap (PBG) properties respond to control of spontaneous emission in quantum devices and light manipulation for photonic information technology [Yablonovitch (1987); Joannopoulos (1997); Lipson (2009); Joannopoulos (2008); Prather (2009)]. PBGs are very sensitive to the periodicity, incident angle and polarizations of the input electromagnetic wave. Moreover, if PBG can reflect electromagnetic wave incident at any incident for both of the TE (Transverse electric) and TM (Transverse magnetic) polarization is known as an omnidirectional band gaps (OBGs). The OBG property has triggered a growing interest to design many potential applications such as omnidirectional reflectors, filters, waveguides and fibers, etc. [Halevi (2000); Dai (2011); Li (2011)]. To make photonic devices that are compact in size, controlled, tunable and robust against disorders, new PBG and OBG mechanism needs to be found. To obtain tunable and controlled PBGs and OBGs, the material properties of one of the constituent materials in the PC structures must depend on some external parameters. Over the last few years, PCs have been intensively investigated with dispersive materials such as metallic materials, semiconductor and metamaterials etc., which material parameters change with frequency, temperature, doping density and magnetic field. Tunable material parameters of dispersive materials are useful to probe and explore PBG phenomena [Nusinsky (2006); Lee (2003)].

In the past decades, several efforts have been dedicated towards the investigation of periodically stacked metamaterials. They have proved to possess novel electromagnetic properties such as negative material properties and negative refraction, super lensing, invisible cloaking and so many. There are mainly two kinds of metamaterials: double-negative (DNG) or negative index materials (NIM) whose permittivity (ε) and permeability (μ) are simultaneously negative, and single negative (SNG) metamaterials, which include the epsilon-negative (ENG) media with negative

permittivity but positive permeability, and the mu-negative (MNG) media with negative permeability but positive permittivity. PC structures with alternating layers of positive index materials (PIMs) and negative index materials (NIMs) lead to a new type of PBG corresponding to zero volume average refractive index is known as zero-<n> gap. Such zero-<n> gap differs fundamentally from a Bragg gap and that is invariant with scaling and insensitive to disorder and independent of the incident angle and polarizations [Li (2003); Vasconcelos (2007); Zhou (2012); Arango (2011)]. Besides NIMs, single-negative materials include the epsilon-negative (ENG) media and the mu-negative (MNG) media have also been attracted researcher's interest. The transmission properties of the 1-D PC containing both kinds of single negative medium shows the possession of a PBG with zero effective phase gap which can be used to realize easily multiple channelled optical filters, where the frequencies of the transmission peaks are almost independent of the incident angles [Jiang (2004); Deng (2010)].

It is accepted incontrovertible the fact that moderately doped semiconductors with low electron density strongly absorb THz radiation and leading to the sensitive change in the transmittance as a function of the dopant level and temperature. Determining the physical properties of doped semiconductor with transient THz radiation has the advantage in THz-imaging, security, spectroscopic analysis, sensing and communications [Isaac (2008); Wang (2010); Bui (2013); Jin (2014)]. These attractive research areas have been extended to introduce semiconductor in PC structures. The use of semiconductors in PCs makes possible the novel tuning of PBGs and OBGs with applied temperature and field, which attractive the feature for sensors and tunable optical device applications [Kong (2011); Zhang (2012); Mehdian (2013); Baryshev (2013)].

In the previous chapters, we have investigated the photonic and omnidirectional band gap and defect mode properties in 1-D GPC structures composed of linear and exponential graded materials. Grading parameters and layer thickness of graded materials in such type GPCs make very different in the behavior from the conventional 1-D PCs and enhance the ability to tune and control of the light wave propagation. Such GPCs play an important role to design spectral filters, detectors, sensors and antireflection coating, etc. Motivated by the possibility to tune and manipulate of the electromagnetic waves by different types of GPCs and dispersive materials such as metamaterials and semiconductor. In this chapter, photonic and Omni-directional band

gap in one-dimensional graded photonic crystal with metamaterials and semiconductor constituents have been presented. Main attention is paid to the influence of structural parameters, grading profile, dispersive materials and temperature on the photonic and Omni-directional band gaps. This work can facilitate the design of filters, reflectors, multichannel filters and sensors, and provide the basic understanding of the influence of graded index materials and dispersive material on the photonic band gap properties in 1-D PCs. The studies have been divided into two parts.

1) Photonic and Omni-directional band gaps of one-dimensional photonic crystals composed of exponential graded index material and metamaterials.
2) Study of photonic band gap properties in one-dimensional graded index photonic crystals with semiconductor.

These sections are arranged as fellows. Initially, the computational model and numerical formulations used for calculation of the reflectance and band structure based on the transfer matrix method have been presented. Next, the reflation spectra, band spectra and omnidirectional band gap at different structural parameters, grading parameters and temperature for the structures have demonstrated. Finally, the results have been summarized.

4.2 Photonic and Omni-directional band gaps of one-dimensional photonic crystal composed of exponential graded index material and metamaterials

4.2.1 Theoretical description

In this section, we have considered a periodic super lattices consisting of alternating layers as ABABAB…. Here, medium 'A' (exponentially graded index material) has thickness d_1, while medium 'B' (metamaterials) has thickness d_2. The exponential graded index material possess the grading refractive index as a function of the depth of layer, whose corresponding dielectric permittivity $\varepsilon_A(\omega)$ and magnetic permeability μ_A are given as

$$\boldsymbol{\varepsilon_A(x) = \varepsilon_i . \exp(\gamma x)\,; \quad \mu_A = 1 \quad \ldots\ldots \quad (4.1)}$$

where $\gamma = \frac{1}{d_1}\log\left(\frac{\epsilon_f}{\epsilon_i}\right)$ is grading parameter, ε_f and ε_i are the lower and higher values of permittivity in the exponential graded index layer, respectively. In the case of

metamaterials as medium B, we consider three different cases. First, the metamaterial possess the negative refractive index in microwave region, whose corresponding electric permittivity $\varepsilon_B(\omega)$ and magnetic permeability $\mu_B(\omega)$ are given by

$$\boldsymbol{\varepsilon_B(\omega) = \ a - \frac{\omega_{ep}^2}{\omega^2}} \text{ and } \boldsymbol{\mu_B(\omega) = \ a - \frac{\omega_{mp}^2}{\omega^2}} \quad \boldsymbol{\ldots\ldots} \quad \textbf{(4.2)}$$

where a and b are positive constants, and ω_{ep} and ω_{mp} are the electronic plasma frequency and magnetic plasma frequency, respectively. In the frequency range of $\omega^2 < \left(\frac{\omega_{ep}^2}{a}, \ \frac{\omega_{mp}^2}{b}\right)$, ε_B and μ_B are negative simultaneously. The physical parameters used here are, a =1.21, b =1 and $\omega_{ep} = \omega_{mp} = 10$ Ghz, motivated by theoretically and experimentally in the previous reports. Secondly, medium B represents the single negative material include the epsilon-negative (ENG) material with negative permittivity equal to $\varepsilon_B(\omega)\ \left(= a - \omega_{ep}^2/\omega^2\right)$ and positive permeability $\mu_B(\omega)$ (= 1.0). In third case, medium B possesses mu-negative (MNG) material with negative permeability equal to $\mu_B(\omega)\ \left(= b - \omega_{mp}^2/\omega^2\right)$ and positive permittivity $\varepsilon_B(\omega)$(= 1.0).

Considered periodic PC structures are in the x-z plane, with periodicity in the x-direction and homogeneity in the z and y. In order to study the properties of electromagnetic waves in this structure, the reflection, transmission, dispersion relation of the periodic super-lattice is obtained by solving the electromagnetic wave equation for s-polarized and p-polarized electromagnetic mode with the layers A and B of the nth unit cell of super-lattice. The component of electric $E_z(x)$ and magnetic $H_y(x)$ field for the nth unit cell have the form as given below for exponential graded index material as layer A and negative index materials as layer B.

For an exponential graded index layer ‘A’;

$$\boldsymbol{E_z(x) = \ A_1 J_0\left(\frac{k_A}{\gamma}\right) + \ B_1 Y_0\left(\frac{k_A}{\gamma}\right)}$$

$$\boldsymbol{H_y(x) = \frac{i}{\omega\mu_A}(-k_A)\left(A_1 J_1\left(\frac{k_A}{\gamma}\right) + \ B_1 Y_1\left(\frac{k_A}{\gamma}\right)\right)} \quad \boldsymbol{\ldots\ldots} \quad \textbf{(4.3)}$$

For a metamaterial layer ‘B’;

$$\boldsymbol{E_z(x) = \ A_2 \exp(-ik_B x) + B_2 \exp(ik_B x)}$$

$$\boldsymbol{H_y(x) = \frac{i}{\omega\mu_B}(-ik_A)[A_2 \exp(-ik_B x) - B_2 \exp(ik_B x)]} \quad \boldsymbol{\ldots\ldots} \quad \textbf{(4.4)}$$

with $k_A = \frac{\omega}{c}\sqrt{\varepsilon_A}\sqrt{\mu_B}\cos\theta_A$ and $k_B = \frac{\omega}{c}\sqrt{\varepsilon_B}\sqrt{\mu_B}\cos\theta_B$, here ω is the angular frequency, c is the velocity of light in vacuum. θ_A, k_A and θ_A, k_B are the refractive angle and wave vectors in the layer A and B, respectively. Then, applying the standard electromagnetic boundary condition at the interface of unit cells, we can find the appropriate transfer matrix for the periodic structure as;

$$\begin{pmatrix} \boldsymbol{A_0} \\ \boldsymbol{B_0} \end{pmatrix} = \boldsymbol{T}\begin{pmatrix} \boldsymbol{A_{2N+1}} \\ \boldsymbol{B_{2N+1}} \end{pmatrix} \text{ and } \boldsymbol{T} = \boldsymbol{M_0^{-1}(M_1M_2)^N M_0} \quad \ldots\ldots \quad \textbf{(4.5)}$$

where N is the number of the unit cells, A_0, B_0, A_{N+1} and B_{N+1} are the electromagnetic field amplitudes of the incident (0^{th}) media and outgoing $(N+1)^{\text{th}}$ media, respectively. Matrices M_0, M_1 and M_2 are 2×2 characteristics matrices of air media, exponential graded index material and metamaterial layers, respectively. Here, the transfer matrix $M_1$and M_2 are given as;

$$\boldsymbol{M_1} = \frac{\boldsymbol{1}}{\Delta}\times\begin{bmatrix} \left\{\boldsymbol{J_0\left(\frac{\xi}{\gamma}\right)_{x=0}.Y_1\left(\frac{\xi}{\gamma}\right)_{x=d_1} - Y_0\left(\frac{\xi}{\gamma}\right)_{x=0}.J_1\left(\frac{\xi}{\gamma}\right)_{x=d_1}}\right\} & \frac{\boldsymbol{1}}{\boldsymbol{q_f}}.\left\{\boldsymbol{J_0\left(\frac{\xi}{\gamma}\right)_{x=d_1}.Y_0\left(\frac{\xi}{\gamma}\right)_{x=0} - J_0\left(\frac{\xi}{\gamma}\right)_{x=0}.Y_0\left(\frac{\xi}{\gamma}\right)_{x=d_1}}\right\} \\ \boldsymbol{q_i}.\left\{\boldsymbol{J_1\left(\frac{\xi}{\gamma}\right)_{x=0}.Y_1\left(\frac{\xi}{\gamma}\right)_{x=d_1} - Y_1\left(\frac{\xi}{\gamma}\right)_{x=0}.J_1\left(\frac{\xi}{\gamma}\right)_{x=d_1}}\right\} & \frac{\boldsymbol{q_i}}{\boldsymbol{q_f}}.\left\{\boldsymbol{J_0\left(\frac{\xi}{\gamma}\right)_{x=d_1}.Y_1\left(\frac{\xi}{\gamma}\right)_{x=0} - J_1\left(\frac{\xi}{\gamma}\right)_{x=0}.Y_0\left(\frac{\xi}{\gamma}\right)_{x=d_1}}\right\} \end{bmatrix}$$

$$\boldsymbol{M_2} = \begin{bmatrix} \boldsymbol{\cos(k_B.d_2)} & \boldsymbol{sin(k_B.d_2)/q_B} \\ \boldsymbol{-q_B\ \sin(k_B.d_2)} & \boldsymbol{\cos(k_B.d_2)} \end{bmatrix} \quad \ldots\ldots \quad \textbf{(4.6)}$$

where $\Delta = \left\{J_0\left(\frac{\xi}{\gamma}\right)_{x=d_1}.Y_1\left(\frac{\xi}{\gamma}\right)_{x=d_1} - Y_0\left(\frac{\xi}{\gamma}\right)_{x=d_1}.J_1\left(\frac{\xi}{\gamma}\right)_{x=d_1}\right\}$, $q_i = \sqrt{\frac{\varepsilon_i}{\mu_i}}.\cos\theta_i$, $q_f = \sqrt{\frac{\varepsilon_f}{\mu_f}}.\cos\theta_f$ and $q_B = \sqrt{\frac{\varepsilon_B}{\mu_B}}.\cos\theta_B$. Here, θ_i and θ_f are the angle at initial and final boundary of the graded layers A. Similarly, we can obtain the characteristic matrix for p-polarized mode with the layers A and B of the unit cell of the super-lattice.

The reflection coefficient of the structure can be obtained by

$$\boldsymbol{r(\omega,\theta)} = \frac{\boldsymbol{(M_{11}+M_{12}P_{N+1})P_0 - (M_{21}+M_{22}P_{N+1})}}{\boldsymbol{(M_{11}+M_{12}P_{N+1})P_0 + (M_{21}+M_{22}P_{N+1})}} \quad \ldots\ldots \quad \textbf{(4.7)}$$

where $P_0 = P_{N+1} = \sqrt{\varepsilon_0/\mu_0}.\cos\theta_0$ for the air media ($\varepsilon_0 = 1, \mu_0 = 1$) of the space x<0 before the incidence end and the space x>L after the exit end, where L is the total

length of the considered periodic structure. $M_{i\,j}(i,j=1,\ 2)$ is the matrix elements of characteristic matrix $M_N(\omega)=(M_1M_2)^N$, which represents the total transfer matrix connecting the field at the incidence and exit ends of the considered structure of the form $(AB)^N$. Matrices M_1 and M_2 are the characteristics matrices for layer A and B, respectively. Thus, the total reflectance can be expressed as;

$$\boldsymbol{R(\omega)=|r(w)|^2} \quad \text{… …} \quad \textbf{(4.8)}$$

Now, the dispersion relation that has been derived for infinite periodic layered medium, according to Bloch's theorem, using the transfer matrix method is

$$\boldsymbol{K(\omega,\theta)=\frac{1}{d}\cos^{-1}\left(\frac{M_{11}+M_{22}}{2}\right)} \quad \text{… …} \quad \textbf{(4.9)}$$

where $M_{11}\ and\ M_{22}$ are the diagonal element of 2×2 translation matrix $(M_1.M_2)$ of a unit cell in the periodic PC structure, d is the length of a period and K is the Bloch wave number. The frequencies at band gap edges are usually found by setting $\cos(Kd)\equiv\pm1$. To propagating the Bloch waves, K should be real and corresponding $|(M_{11}+M_{22})/2|\leq1$. Spectral bonds within which K is complex correspond to evanescent wave that are rapidly attenuated and defined by the condition $|(M_{11}+M_{22})/2|>1$. These bands correspond to the stop band also called PBGs or forbidden gaps since propagating modes do not exist for the systems. After simplify the equation (4.9), the dispersion relation also can be written as;

$$\begin{aligned}\cos(Kd)&=\frac{1}{2}\sqrt{\frac{z_f}{z_i}}.\left[\frac{4}{3}.\cos(z_f-z_i)\cos(k_B.d_2)-\left(\frac{q_i}{q_1}+\frac{q_1}{q_f}\right).\sin(z_f-z_i)\sin(k_B.d_2)\right]\\&=\sqrt{\frac{z_f}{z_i}}.\left[\frac{2}{3}.\cos(z_f-z_i+k_B.d_2)-\frac{1}{2}\left(\frac{q_i}{q_1}+\frac{q_1}{q_f}-\frac{4}{3}\right).\sin(z_f-z_i)\sin(k_B.d_2)\right]\end{aligned} \quad \text{… …} \quad \textbf{(4.10)}$$

where $z_f=\left(\frac{\xi}{\gamma}\right)_{x=d_1}$ and $z_i=\left(\frac{\xi}{\gamma}\right)_{x=0}$. It can clearly see that the first term in above equation represent the solution in an inhomogeneous medium with average refractive index $\bar{n}=\left[(n_f-n_i)d_1+n_Bd_2\right]/d$, and the second term is responsible for gap opening if there is an impedance mismatch. For the periodic multilayer structures consisting of homogeneous positive index and negative index materials, the $\bar{n}=0$ band gaps occur when the incident wave frequency located at cos(Kd)=1. The zero-$\bar{n}$ gap can be regard as the zero-th order Bragg gap. The uniqueness of such a special Bragg gap is that the phase accumulation of a wave passing through the scaled unit cell is still zero, which ensures the gap opening condition satisfied for the scaled system. Such property

only exists in a composite medium with positive and negative refractive index components, so that phase accumulations through different parts can exactly cancel each other. Apparently, such phase cancellation is insensitive to rescaling the whole structure, which is not the case for a conventional Bragg gap. However, zero-$\bar{n}$ band gap condition is not satisfied in our considered structures with exponential graded index-negative index materials because at $\bar{n} = 0$, $\cos(Kd) \neq 1$, and the phase accumulation of a wave passing through the particular scaled unit cell is also zero i.e. exactly cancel each other but such phase cancellation is sensitive to the scaling of the structure. Because, our structures consist simultaneously space and frequency dependent refractive index materials layer, so band gap at $\bar{n} = 0$ is not distinct from a conventional Bragg gap.

4.2.2 Numerical results and discussion

In this section, we present some numerical results to characterize the optical reflection, band structures and omnidirectional band gap due to the exponential graded index material-metamaterial periodic PC structures. We consider medium A as exponential graded materials with permittivity ε_A and permeability μ_B; while medium B (metamaterials) have the frequency dependent dielectric function $\varepsilon_B(\omega)$ and permeability $\mu_B(\omega)$ given according to three different cases: first, medium B as negative index material and then medium B represents as a single negative material includes a epsilon-negative (ENG) material with negative permittivity and positive permeability and finally, medium B assumes as mu-negative (MNG) material with negative permeability and positive permittivity. Our results observation according to the structure with different metamaterials has been carried out in three parts.

4.2.2.1 Structure with negative index (ε<0, μ<0) material

We first present the reflection and photonic band gap spectra of 1-D periodic system composed by exponential graded index and negative index (ε<0, μ<0) materials at different layer thickness (given in the caption of figures) under normal incident angle and show in panels a(i-v) and b(i-v) of the figure 4.1, respectively. Figures show the dependence of the PBGs on the lattice constant. The dark areas in the panel (b) of the figure are the PBG regions. The number of PBGs increases with increase of the thickness of negative index material layers (B), while graded layers (A) thickness d_1 is fixed and equal to 16 mm. Edges of band gaps shift from lower to higher frequency and

new narrow and narrow band gaps appear with increasing the thickness of layer B. The geometrical size of the whole structure and lattice constant affect the number of PBGs and their band region (See figure 4.1). The band structure in panel (b) and the reflectance in panel (a) of the figure 4.1 clearly show the formation of band gaps with variation of the thickness of layer B. The $< \tilde{n} >$ (effective refractive index of graded index and negative index materials layers) of our system is zero at the frequency 5.845 GHz for $d_1 = 16\ mm$ and $d_1 = 24\ mm$, and a gap can be opened at that frequency, but the second term in the dispersion relation is not zero due to mismatch impedance. Therefore the dispersion relation equation (4.10) has no unique solution for K = 0 at $< \tilde{n} >= 0$, which indicating a zero gap. Similarly, the $< \tilde{n} >$ of the considered system is also zero at frequency 5.525 GHz, 5.115 GHz, 4.59 GHz and 3.91 GHz for $d_1 = 16\text{mm}$ and $d_2 = 20$ mm, 16 mm, 12 mm, and 8 mm, respectively. These zero-$\tilde{n}$ frequencies exist inside the Bragg band for normal incidence. A Bragg gap is an intrinsic consequence of periodicity and the gap frequency is tied with the size of unit-cell. Therefore, Bragg gaps position change with the size of unit-cell, and which are demonstrated in figure 4.1.

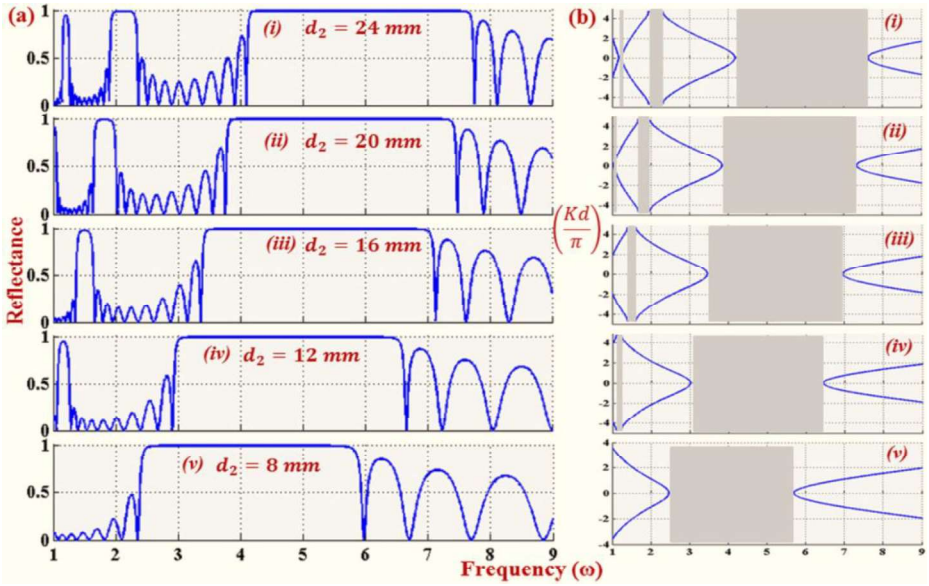

Figure 4.1 (a) Reflectance and (b) band structure of the structure with alternating layers of exponential graded index material (16 mm thick) and the negative index material (thickness d_2) at normal incidence. Panels (i), (ii), (iii), (iv) and (v) are for the thicknesses d_2 equal to 24 mm, 20 mm, 16 mm, 12 mm and 8 mm, respectively.

For better understanding of the effect of layer thickness on the PBGs in the proposed structure, we have depicted the variation of PBGs in the figure 4.2. This figure shows the dependence of PBGs on the ratio of thickness of two media at normal

incidence under different lattice constant (a) $d_1 = 24$ mm (b) $d_1 = 20$ mm and (c) $d_1 = 12$ mm. It can clearly see that the lower and higher edges of band gaps are affected by the ratio of layer thickness and shifted towards higher frequency with increase of the ratio (d_2/d_1), and the gap II and III are emerge. The band width of gaps increases with increasing the ratio of layer thickness in all cases. Gap-I have wider bandwidth but gap II and III have narrow bandwidth. The values of graded layer thickness influence on the bandwidth and frequency region of the gaps but metamaterial layer thickness influences on the frequency region, bandwidth and formation of the PBGs.

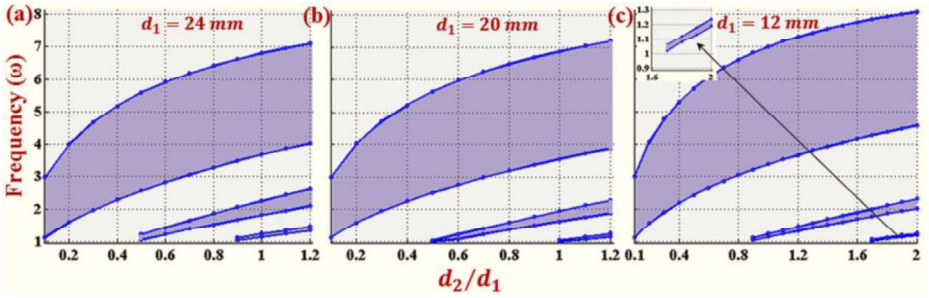

Figure 4.2 The dependence of photonic band gaps on the ratio of thickness of graded index and negative index materials layer under three different lattice constants (a) d_1 = 24 mm, (b) d_1 = 20 mm and (c) d_1 = 12 mm of the structures at normal incidence.

Now, the dependence of PBGs on the ratio of initial (ε_i) and final (ε_f) permittivity i.e $(\varepsilon_f/\varepsilon_i)$ of the exponential graded index layers have investigated. Here, initial permittivity (ε_i) is assume to fixed and equal to 2.25, while final permittivity (ε_f) varies according to the ratio$(\varepsilon_f/\varepsilon_i)$. The reflection spectra for the different values of $(\varepsilon_f/\varepsilon_i)$ in the periodic $(AB)^{10}$ structures with layers thickness (a) d_1 = 24 mm and d_2 = 28 mm (b) d_1 = 18 mm and d_2 = 28 mm, and (c) d_1 = 24 mm and d_2 = 18 mm have depicted in figure 4.3. As expected, the photonic bandwidth decreases with decreasing the $(\varepsilon_f/\varepsilon_i)$ values. The explanation of this phenomenon is that decreasing the ratio-values, the rate of modification of the grading profile parameter (γ) decreases and corresponding average refractive index over the volume of each graded layer conjointly decreases, hence influence of the Bragg stack become less effectively. When the thickness of graded layers decreases and of meta-material layers is constant, band gaps slightly shifted towards higher frequency range and their band width decreases, but number of band gaps is same. However, thickness of meta-material layers decreases and of graded layers is constant, the band gaps edges shifted towards lower frequency and their band width decreases and number of band gaps also decreases. In other words, the values of

d_1 influence on the width and frequency range of the PBG, but the values of d_2 influence on the width, frequency range and number of the PBG.

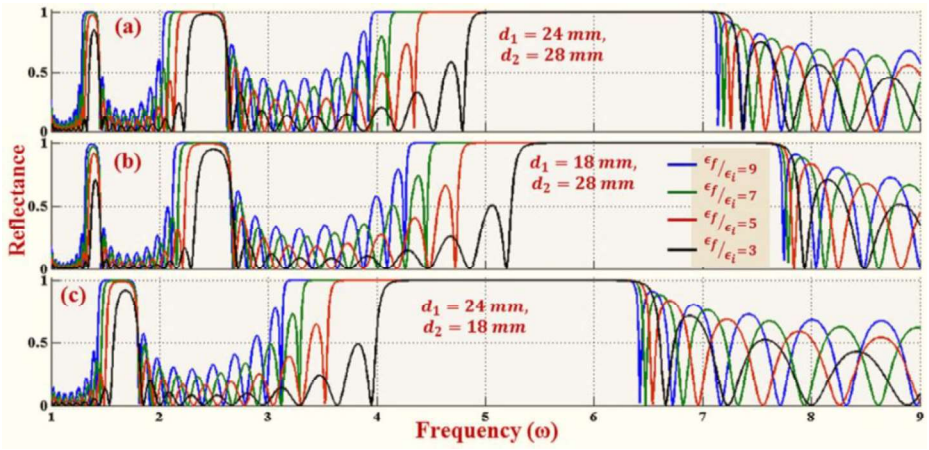

Figure 4.3 Panels (a) d_1 = 24 mm, d_2 = 28 mm, (b) d_1 = 18 mm, d_2 = 28 mm and (c) d_1 = 24 mm, d_2 = 18 mm show the reflection spectra as a function of the ratio $(\boldsymbol{\varepsilon_f/\varepsilon_i})$.

To have a more complete description and a better understanding of the effect of the contrast of initial and final permittivity of the graded index layers on the PBG characteristics, we have plotted the photonic bands (shaded areas) as a function of the $(\varepsilon_f/\varepsilon_i)$ in the case of the layers thickness (a) d_1 = 24 mm and d_2 = 28 mm, (b) d_1 = 18 mm and d_2 = 28 mm, and (c) d_1 = 24 mm and d_2 = 18 mm in figure 4.4. As expected, photonic band gap increases with increasing the values of $(\varepsilon_f/\varepsilon_i)$.

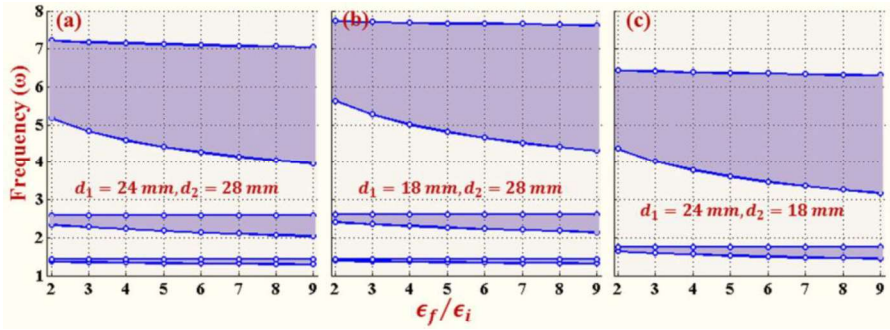

Figure 4.4 The dependence of the photonic band gaps on the ratio $(\boldsymbol{\varepsilon_f/\varepsilon_i})$ under three different lattice constants (a) d_1 = 24 mm, d_2 = 28 mm, (b) d_1 = 18 mm, d_2 = 28 mm and (c) d_1 = 24 mm, d_2 = 18 mm for the structure.

The dependence of PBGs on the incident angle in the structure with layers thickness d_1 = 24 mm and d_2 = 28 mm for TE and TM polarization are shown in figures 4.5(a) and 4.5(b). These figures are clearly demonstrated the expansion of PBGs for both TE and TM-wave, when the incident angle increases. In order to discuss the OBG properties of the structures, we have plotted the projection band structures as changing

of the incident angle and exhibited in figure 4.5(c). From this figure, we can clearly inspect the variation of higher and lower band edges as changing the angle of incident. There is OBGs, which exist between higher and lower band gap edges as prevent band gap region for both TE and TM-polarization. In figure 4.5(c), the dark areas represent the forbidden band for relative polarization and the ubiquitous white areas between the band edges in both polarizations illustrated the OBGs.

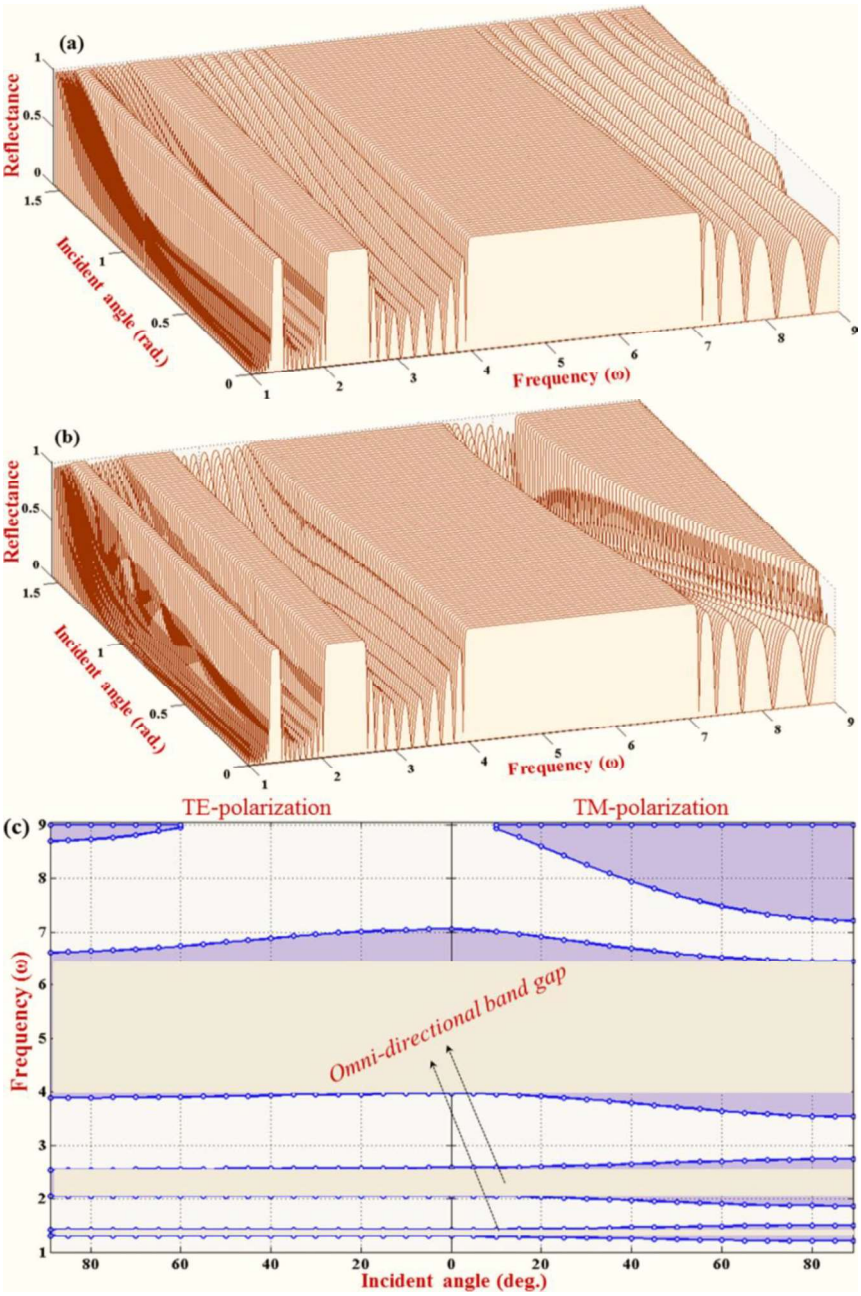

Figure 4.5 Reflection spectra for (a) TE-polarization, (b) TM-polarization and (c) projected reflection band structure as changing of the incident angle in the structure with lattice constant $d_1 = 24$ mm and $d_2 = 28$ mm.

Gap I and II lie in the single frequency range for TE-mode while the frequency range slightly expanded with angle for TM-mode, gap III and IV are out of the single frequency range. Gap IV is appear due to breaking of the Snell's law, when refractive index exist between 0 and 1, that is to say that no real solution obtain for any refraction angle $\theta_{(A \text{ or } B)}$ of the equation $\sin\theta = n_{(A\,or\,B)} \sin\theta_{(A\,or\,B)}$, under the incident angle ($\theta \neq 0$). Furthermore, we have emphasized the OBGs as changing of the thickness ratio d_2/d_1 for the structures with fixed exponential graded layer thickness (a) $d_1 = 24$ mm, (b) $d_1 = 16$ mm and (c) $d_1 = 8$ mm, and shown in figure 4.6. The OBG increases and shifted toward high frequency with increasing the value of d_2/d_1, but that slightly decreases at higher ratio as illustrated in the figures 4.6(a - c). Here, we can also clearly see that the values of d_1 only influence on the width of OBGs, but the values of d_2 influence both bandwidth and number of OBGs.

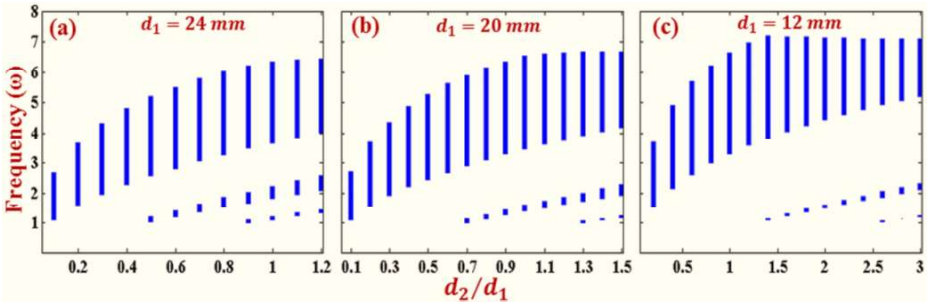

Figure 4.6 The distribution of the Omni-directional bandwidths as a function of the ratio of the thickness of graded and negative index materials under three different lattice constants (a) $d_1 = 24$ mm, (b) $d_1 = 16$ mm and (c) $d_1 = 8$ mm for the considered structures.

Accordingly, the bandwidth and frequency range of the photonic and Omni-directional band gaps can be changed by thickness and grading profile parameter of the graded layers. Thickness of meta-material layer also affected the bandwidth, band gap region and number of the photonic and Omni-directional band gaps. Band gap decreases with the thickness of metamaterial layers. Thus, photonic and omnidirectional band gap can be modulated by structural and material parameters of the considered structures.

4.2.2.2 Structure with epsilon-negative (ε<0, μ=1.0) material

Here, the PBG and OBG properties for different structural and material parameters in the periodic structure consists of exponential graded index material as layer 'A' and epsilon-negative (ε<0, μ=1) material as layer 'B' are demonstrated. The dependence of the reflection band gap on the thickness of layer B (given in the figure) under normal incident angle are shown in figure 4.7. It can be seen that two band gaps

form for such type structures and their bandwidth decreases with the thickness of epsilon-negative material layers (B), while graded layers (A) thickness d_1 is fixed and equal to 24 mm. Band edges of first band gap shift toward lower frequency while edges of second band gap toward higher frequency. Bandwidths of first and second bands are approximately equal for layer thickness $d_1 = 24$ mm and $d_2 = 40$ mm, but for other value of d_2, bandwidth of second band slightly decreases as compare to first band with decreasing the value of d_2. Accordingly, this structure can be used to deign pass band optical filters.

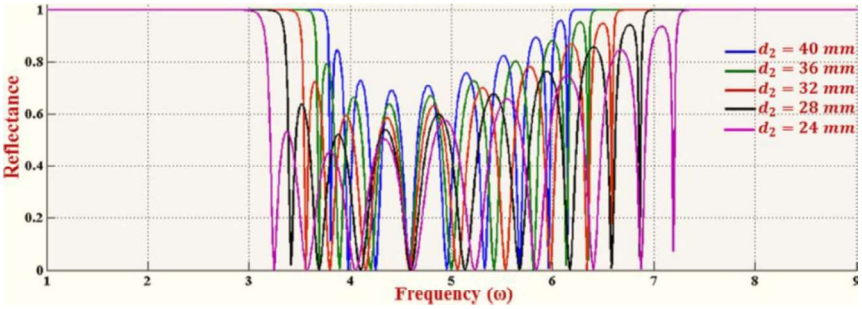

Figure 4.7 Reflectance for the structure with alternating layers of exponential graded index material (24 mm thick) and the epsilon-negative material (thickness d_2) at normal incidence. Panels (a), (b), (c), (d) and (e) are for different values of thickness d_2 equal to 40 mm, 36 mm, 32 mm, 28 mm and 24 mm, respectively.

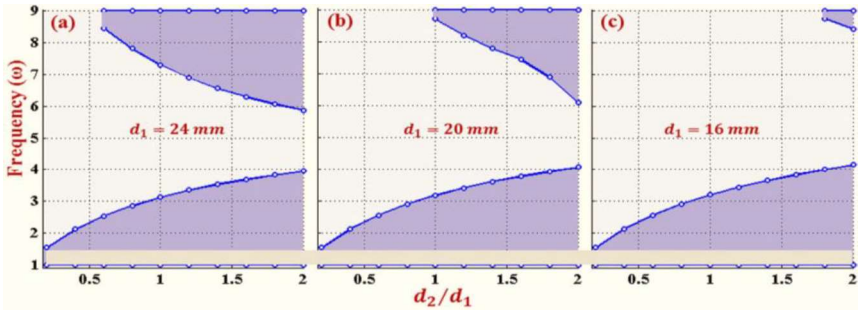

Figure 4.8 The dependence of PBGs on the ratio of the thickness of graded and epsilon-negative materials layers under three different lattice constants (a) $d_1 = 24$ mm, (b) $d_1 = 20$ mm and (c) $d_1 = 16$ mm in the considered structure at normal incidence.

Furthermore, the dependence of bandwidth on the ratio (d_2/d_1) at normal incidence under different lattice constant (a) $d_1 = 24$ mm (b) $d_1 = 20$ mm and (c) $d_1 = 16$ mm is shown in figure 4.8. It can clearly see that the upper and lower edges of first and second bands are affected by the ratio of layers thickness. The upper and lower edges of first and second bands are shifted towards higher and lower frequency side, respectively with increase of the ratio (d_2/d_1). Comparing the figures 4.8(a), 4.8(b) and 4.8(c), we find that the bandwidth of the gaps depends on the ratio of the layer thickness and that increases with increasing the value of d_2. The formation of first band and their

bandwidth are approximately same but formation of second band shifted toward higher values of ratio (d_2/d_1) and their bandwidth decreases with the values of d_1. The values of graded layers thickness influences the formation and bandwidth of second band while first band is insensitive, while meta-material layers thickness influences on both first and second band gaps. We observe that the geometrical size of the whole structure and the lattice constant affect the bandwidth and position of band gap edges and it is clearly demonstrated in the figures 4.7 and 4.8.

Now, the dependence of PBG on the ratio of initial (ε_i) and final (ε_f) permittivity i.e $(\varepsilon_f/\varepsilon_i)$ of the graded layers is demonstrated. Here, initial permittivity (ε_i) is equal to 2.25, while final permittivity (ε_f) varies according to $(\varepsilon_f/\varepsilon_i)$-value. In the figure 4.9, the reflection spectra for different $(\varepsilon_f/\varepsilon_i)$-values in the periodic $(AB)^{10}$ structures with layers thickness (a) $d_1 = 24$ mm and $d_2 = 40$ mm (b) $d_1 = 18$ mm and $d_2 = 40$ mm, and (c) $d_1 = 24$ mm and $d_2 = 28$ mm are depicted.

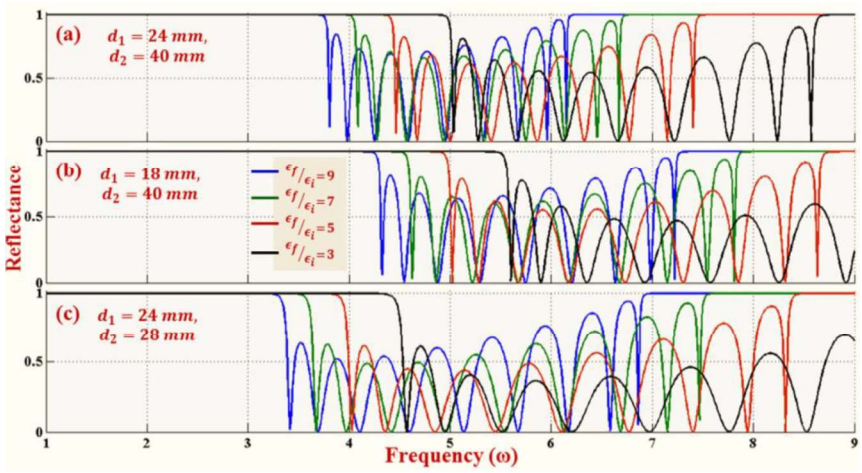

Figure 4.9 The reflection spectra as a function of the ratio $(\varepsilon_f/\varepsilon_i)$ show in panels (a) $d_1 = 24$ mm, $d_2 = 40$ mm, (b) $d_1 = 18$ mm, $d_2 = 40$ mm and (c) $d_1 = 24$ mm, $d_2 = 28$ mm.

As expected, the bandwidth of band gaps decreases with $(\varepsilon_f/\varepsilon_i)$-value. Comparing the figures 4.9(a) and 4.9(b), band edges of band gaps shifted towards higher frequency range and bandwidth of first gap increases when thickness of graded layers decrease and thickness of epsilon-negative material layers to be constant, while bandwidth of second band gap decreases with increasing the $(\varepsilon_f/\varepsilon_i)$-value, and finally second band disappears at higher $(\varepsilon_f/\varepsilon_i)$-values. However, comparing the figures 4.9(a) and 4.9(c), we get the formations of band gaps are same, but bandwidths of first and second band gaps become change when thickness of metamaterial layers decreases and thickness of

graded layers to be constant. In other words, the values of both d_1 and d_2 influence on the bandwidth and frequency range of the photonic bands. To have a more complete description and a better understanding of the effect of $(\varepsilon_f/\varepsilon_i)$-value on the PBG characteristics, the formation of photonic bands (shaded areas) as a function of the $(\varepsilon_f/\varepsilon_i)$ in the case of layers thickness (a) $d_1 = 24$ mm and $d_2 = 40$ mm, (b) $d_1 = 18$ mm and $d_2 = 40$ mm, and (c) $d_1 = 24$ mm and $d_2 = 28$ mm is plotted the figure 4.10. One clearly sees that PBG increases with increasing the $(\varepsilon_f/\varepsilon_i)$-values.

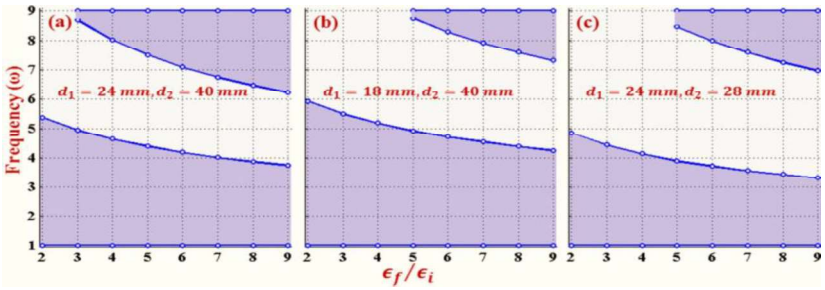

Figure 4.10 The dependence of the photonic band gaps on the ratio $(\varepsilon_f/\varepsilon_i)$ under three different lattice constants (a) $d_1 = 24$ mm, $d_2 = 40$ mm, (b) $d_1 = 18$ mm, $d_2 = 40$ mm and (c) $d_1 = 24$ mm, $d_2 = 28$ mm of the structure.

The dependence of photonic band gaps on the incident angle in the considered structure with layer thickness $d_1 = 24$ mm and $d_2 = 40$ mm for TE and TM polarization has been shown in figure 4.11(a) and 4.11(b). These figures are clearly demonstrated the expansion of photonic band gaps for both TE and TM-wave, when the incident angle increases. In order to discuss the OBG properties of the structures, we have plotted the projection band structures as changing of the incident angle in figure 4.11(c). From this figure, we can clearly inspect the variation of higher and lower band edges as changing the angle of incident. OBGs exist between higher and lower band gap edges as prevent band gap region for both TE and TM-polarization. In figure 4.11(c), the dark areas represent the forbidden band for relative polarization and the ubiquitous white areas between the band edges in both polarizations depicted the OBGs. Frequency ranges of both bands are slightly expanded with incidence angle for TE-mode, while frequency range of first band reduces and frequency range of second band spreads with incidence angle for TM-mode. Furthermore, we have emphasized the OBGs as changing of the thickness ratio d_2/d_1 for the structures with fixed exponential graded index layers thickness (a) $d_1 = 24$ mm, (b) $d_1 = 20$ mm and (c) $d_1 = 16$ mm. The bandwidth of OBGs increases with the value of d_2/d_1 i.e. increasing the thickness of epsilon-negative material layers as illustrated in figure 4.12.

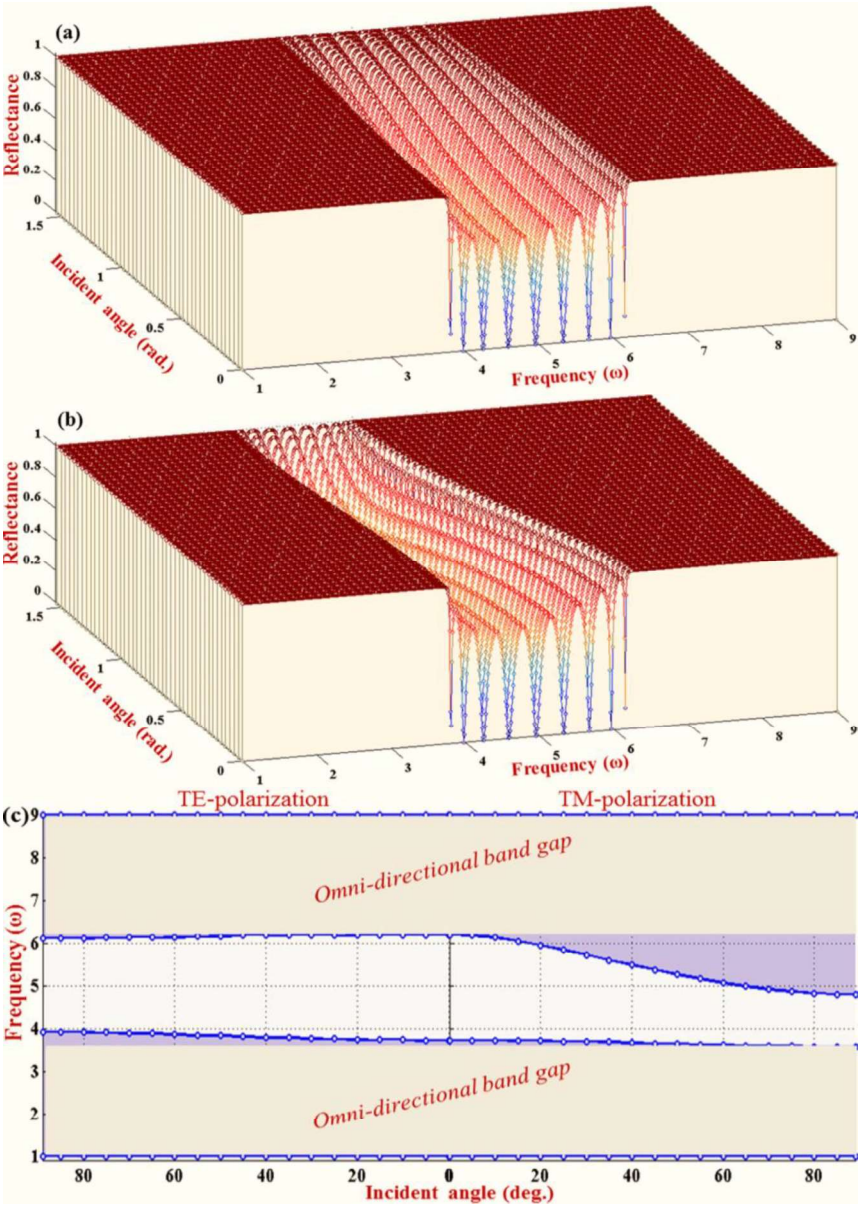

Figure 4.11 Reflection spectra for (a) TE-polarization, (b) TM-polarization and (c) projected reflection band structure as changing of the incident angle in the structure with lattice constant $d_1 = 24$ mm and $d_2 = 40$ mm.

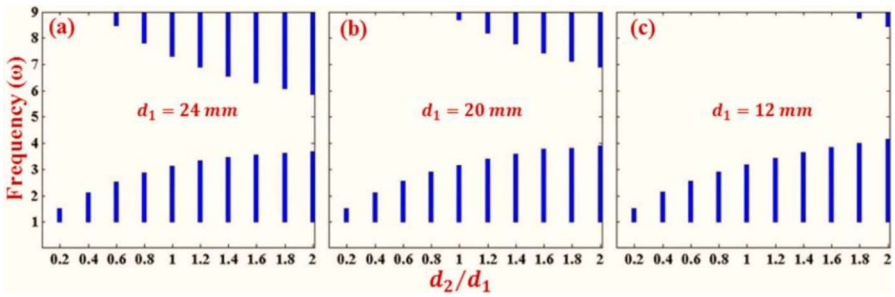

Figure 4.12 The distribution of the Omni-directional bandwidths as a function of the ratio of the thicknesses of graded and epsilon-negative materials under three different lattice constants (a) $d_1 = 24$ mm, (b) $d_1 = 20$ mm and (c) $d_1 = 16$ mm for the structure.

The bandwidth of first omnidirectional bands increases and bandwidth of second omnidirectional bands decrease, when the graded layer thickness increases, but their generation shift to higher frequency side with increasing the values of d_2/d_1, as depicted in the figures 4.12(a - c). The values of both d_1 and d_2 influence the bandwidth and formation of the OBGs.

According to the above results, two photonic and Omni-directional band gaps are obtain in the proposed structure. Band gaps can be control by layer thickness and grading profile parameter of the graded layers. These structures can be used to design pass band optical filters with tunable band range.

4.2.2.3 Structure with mu-negative (ε=1, μ<1) materials

In this section, the PBG and OBG properties for different lattice parameters in the periodic structure composed of exponential graded index material as layer 'A' and mu-negative (ε=1, μ<1) material as layer 'B' have presented. First, the dependence of the reflection bands on the thickness of layer B (given in the figure) under normal incident angle has shown in figure 4.13. A single broader band gap observe for the structure and their bandwidth decreases with the thickness (d_2) of mu-negative material layers (B), while graded layers (A) thickness d_1 is fixed and equal to 16 mm.

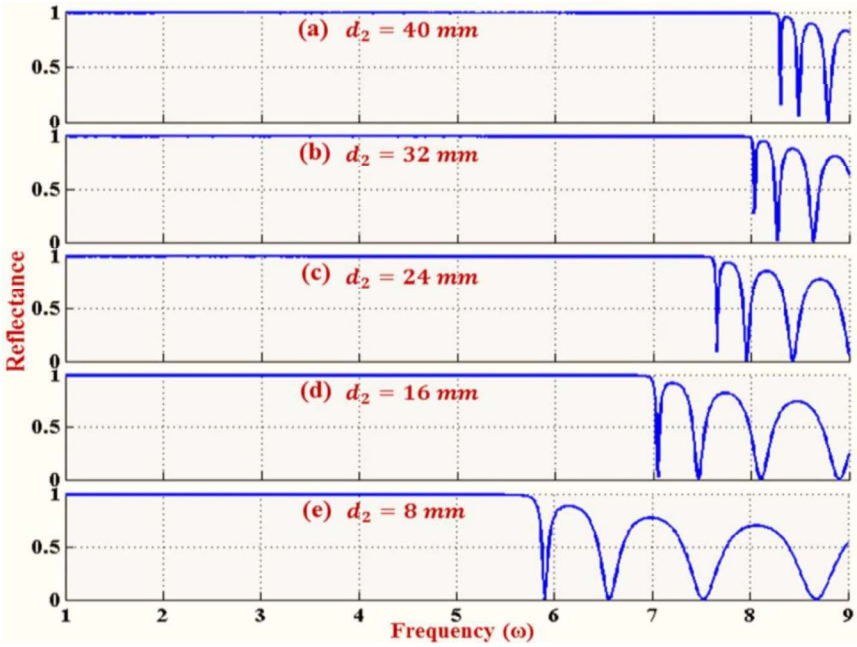

Figure 4.13 Reflectance spectra for the structure with alternating layers of exponential graded index material (16 mm thick) and mu-negative material (thickness d_2) at normal incidence. Panels (a), (b), (c), (d) and (e) are the reflectance spectra for the thickness d_2 equal to 40 mm, 32 mm, 24 mm, 16 mm and 8 mm, respectively.

Furthermore, the dependence of PBG on the ratio (d_2/d_1) under normal incidence at different lattice constant (a) $d_1 = 24$ mm (b) $d_1 = 20$ mm and (c) $d_1 = 12$ mm has been demonstrated in figure 4.14. We can clearly see that only the upper edge of band gap is affected by the ratio of layer thickness. The upper edge of bands shifted towards higher frequency and bandwidth increases, with increase of the ratio (d_2/d_1). Comparing the figures 4.14(a), 4.14(b) and 4.14(c), we find that the bandwidth of the gap increases with the ratio of layer thickness for different fixed values of d_1. The values of graded layer thickness has moderately influenced on the bandwidth, while single negative material layer thickness has extensively affected on the bandwidth of band gaps (See in the figures 4.13 and 4.14).

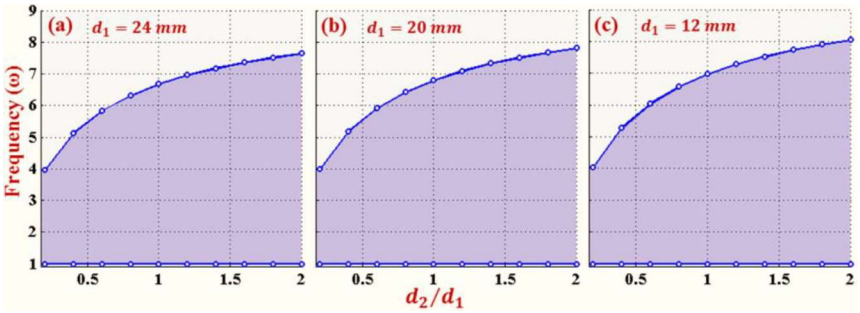

Figure 4.14 The dependence of the photonic band gaps on the ratio of the thickness of graded index and mu-negative materials under three different lattice constants (a) $d_1 = 24$ mm, (b) $d_1 = 20$ mm and (c) $d_1 = 12$ mm of the structure at normal incidence.

Now, we evince the effect of the ratio of initial (ε_i) and final (ε_f) permittivity i.e $(\varepsilon_f/\varepsilon_i)$ of the exponential graded index layer on the PBG. Here, initial permittivity (ε_i) equal to 2.25, while final permittivity (ε_f) varies according to $(\varepsilon_f/\varepsilon_i)$-values. In the figure 4.15, we have depicted the reflection spectra for various $(\varepsilon_f/\varepsilon_i)$-values in the periodic structure $(AB)^{10}$ with layer thickness (a) $d_1 = 20$ mm and $d_2 = 24$ mm (b) $d_1 = 16$ mm and $d_2 = 24$ mm, and (c) $d_1 = 20$ mm and $d_2 = 16$ mm. As expected, the bandwidth of band gaps decreases with the $(\varepsilon_f/\varepsilon_i)$-values, but the effect of grading parameter on band gap is marginally. Comparing the figures 4.15(a) 4.15(b) and 4.15(c), the edge of band gaps shifted towards higher frequency range and bandwidth increases when thickness of graded index layers decrease and thickness of mu-negative material layers to be constant, while the grading profile parameter has no considerable effect on the band gap. The formations of band gaps are same for all cases and their bandwidth decreases when thickness of mu-negative material layer decreases. To have a more complete description of the effect of $(\varepsilon_f/\varepsilon_i)$-values on the PBG characteristics,

the variations of photonic band (shaded areas) as a function of $(\varepsilon_f/\varepsilon_i)$-values in the case of the structure with layer thickness (a) d_1 = 20 mm and d_2 = 24 mm, (b) d_1 = 16 mm and d_2 = 24 mm, and (c) d_1 = 20 mm and d_2 = 16 mm are plotted in the figure 4.16. One clearly sees that PBG narrowly decreases with increasing the $(\varepsilon_f/\varepsilon_i)$-values, while band gap significantly change with changing the thickness of graded index and mu-negative material layers.

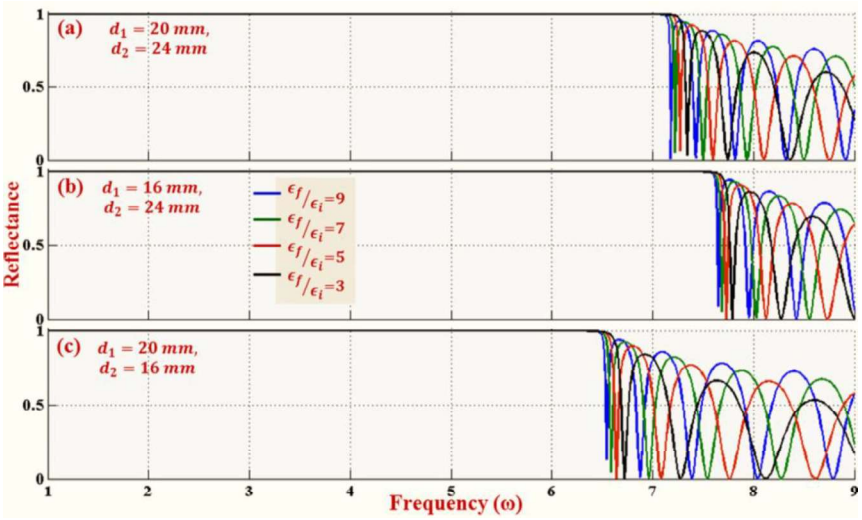

Figure 4.15 Reflection spectra as a function of the ratio $(\varepsilon_f/\varepsilon_i)$ show in panels (a) d_1 = 20 mm, d_2 = 24 mm, (b) d_1 = 16 mm, d_2 = 24 mm and (c) d_1 = 20 mm, d_2 = 16 mm.

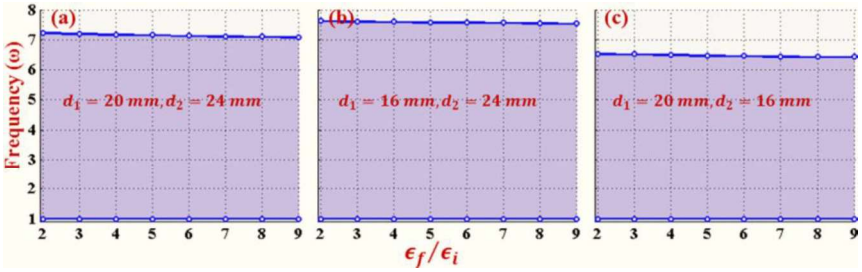

Figure 4.16 The dependence of PBG on the ratio $(\varepsilon_f/\varepsilon_i)$ under three different cases of the lattice parameter (a) d_1 = 20 mm, d_2 = 24 mm, (b) d_1 = 16 mm, d_2 = 24 mm and (c) d_1 = 20 mm, d_2 = 16 mm for the considered structure.

The dependence of PBG on the incident angle in the proposed structure with layer thickness d_1 = 24 mm and d_2 = 40 mm for TE and TM polarization are shown in the figures 4.17(a) and 4.17(b), respectively. These figures are clearly demonstrated the expansion of PBG for both TE and TM-wave, when the incident angle increases. In order to discuss the OBG properties of the structures, we have plotted the projection band structure as changing of the incident angle in figure 4.17(c). From this figure, we can clearly inspect the variation of higher and lower band edges as changing the angle

of incident. Frequency range of band gap slightly reduces with angle for TE-mode, while it expands with angle for TM-mode. An OBG exist between higher and lower band gap edges as prevent band gap region for both TE and TM-polarization. In figure 4.17(c), the dark areas represent the forbidden band for relative polarization and the ubiquitous white area between the band edges in both polarizations exhibits the OBG.

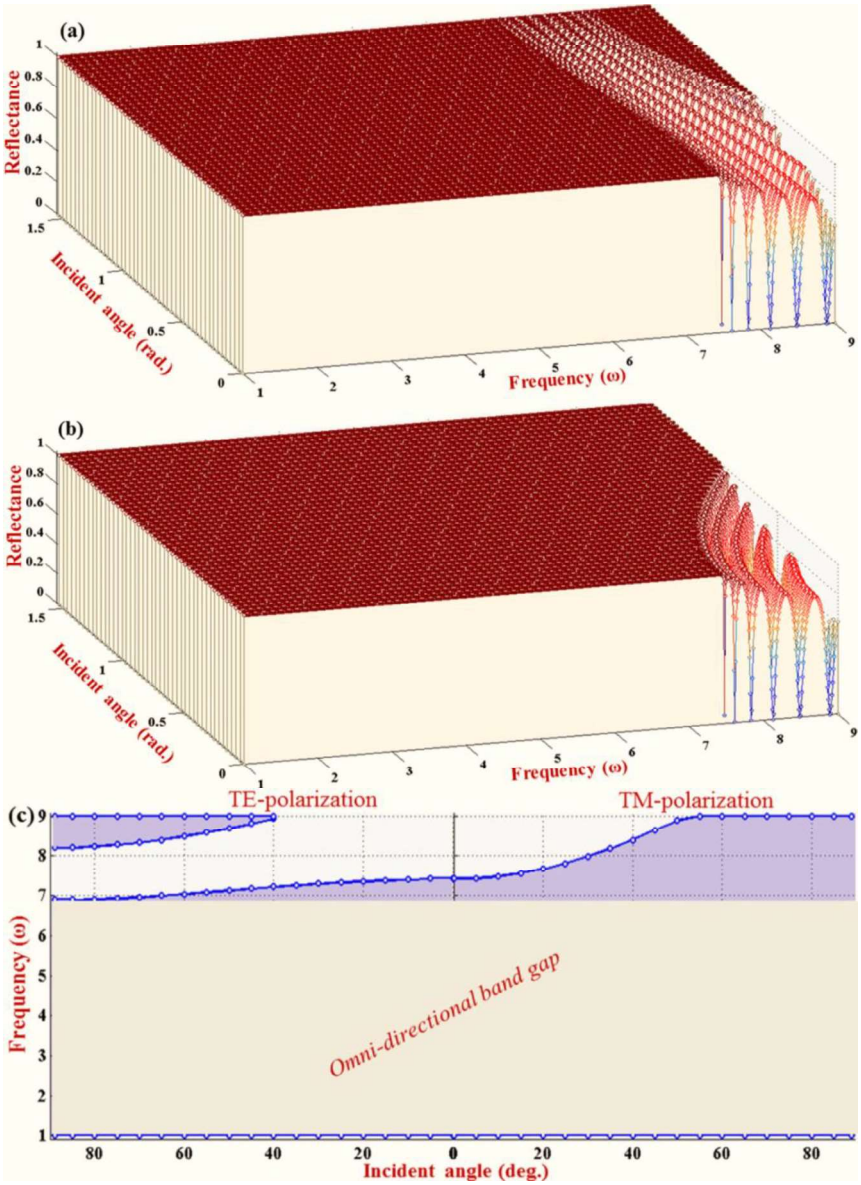

Figure 4.17 Reflection spectra for (a) TE-polarization, (b) TM-polarization and (c) projected reflection band structure as changing of the incident angle in the structure with lattice parameter $d_1 = 24$ mm and $d_2 = 40$ mm.

Furthermore, we have emphasized the OBG as changing of the thickness ratio d_2/d_1 for the structure with fixed exponential graded index layer thickness (a) $d_1 = 24$ mm, (b) $d_1 = 20$ mm and (c) $d_1 = 16$ mm. The bandwidth of OBG increases with

increasing the value of d_2/d_1 i.e. increasing the thickness (d_2) of mu-negative material layer as shown in the figure 4.18. The width of omnidirectional band also slightly increases with decrease of the graded layer thickness as clearly demonstrated in the figures 4.18(a), 4.18(b) and 4.18(c). The values of both layers thickness d_1 and d_2 influence on the width of the OBG.

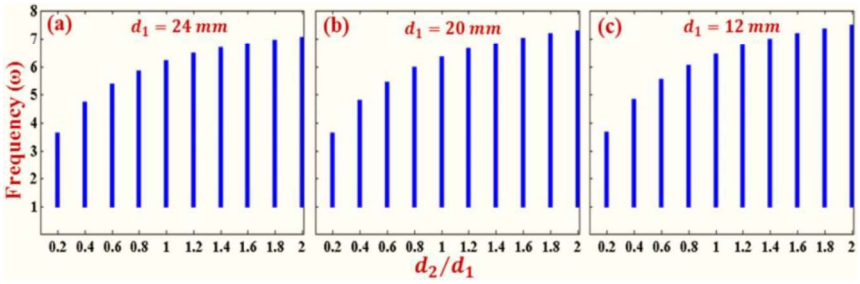

Figure 4.18 The distribution of the Omni-directional bandwidths as a function of the ratio of the thickness of graded and mu-negative materials under three different lattice parameters (a) $d_1 = 24$ mm, (b) $d_1 = 20$ mm and (c) $d_1 = 16$ mm of the structures.

In these types of structures, we obtain single large bandwidth photonic and omnidirectional band gaps and their band width can be control by layer thickness of the structure. These structures can be used to design low pass optical band filters with tunable frequency range.

4.3 Study of photonic band gap properties in one-dimensional graded index photonic crystals with semiconductor

4.3.1 Theoretical description

In this section, we have considered a periodic structure $(AB)^P$, where A and B represent two kinds of dielectric layers and P is the number of periods. One is the graded index layer (A) with varying refractive index as a function of the layer thickness and the other is semiconductor material layer (B) with frequency and temperature dependent refractive index. The schematic view of the structure is shown in figure 4.19(a). Refractive index profile in the considered graded layers varies in two different ways with layer thickness. First, index of refraction varies exponentially from initial to the end boundary of the graded layer and is represented as; [Yeh, 1988].

$$n_{AE}(x) = n_i \exp\left(\frac{x}{d_1} \ln \frac{n_f}{n_i}\right) \quad \ldots\ldots \quad (4.11)$$

In second case, refractive index varies linearly from initial to the final boundary of the graded layer, which can be expressed as;

$$n_{AL}(x) = n_i + \frac{n_f - n_i}{d_1} x \quad \ldots\ldots \quad (4.12)$$

where n_i and n_f is the initial and final refractive index at the boundary of the graded layers, respectively and d_1 is the layer thickness. The variations of the optical index n_A for exponential and linear graded index layer are shows in the figure 4.19(b).

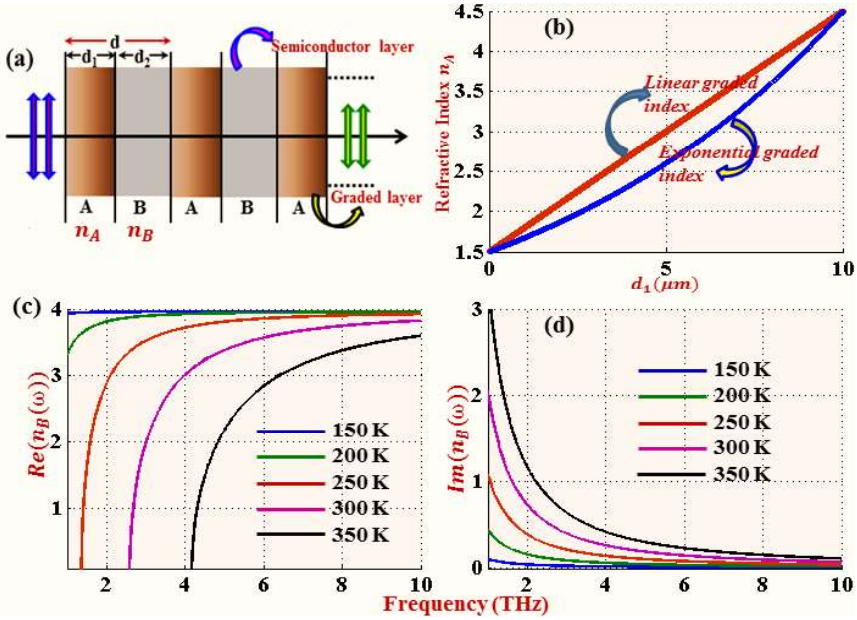

Figure 4.19 (a) Schematic diagram of the considered structure constituted with graded index layers as A (linear and exponential graded index materials) and semiconductor material layers as B, the background medium is air. (b) Refractive index variation in a graded layer as a function of layer thickness d_1 (here, d_1 = 10 μm). (c) and (d) are the real and imaginary part of the refractive index of the semiconductor (InSb) as a function of frequency with the varying temperature. The parameters are $\boldsymbol{\varepsilon_\infty = 15.68}$, $\boldsymbol{m^* = 0.015 m_e}$, $\boldsymbol{m_e = 9 \times 10^{-31} kg}$ and γ = 2π × 0.05 THz.

In this section, we choose the semiconductor InSb with a surface plasma frequency (ω_p) in the THz range as the components of the 1-D PCs to investigate the PBG in terahertz frequency range. Semiconductor InSb have remarkably tunable dielectric constant as a function of temperature. Dielectric function of InSb at THz frequency is similar to the dielectric function of metals at visible-ultraviolet frequencies. The dielectric function of InSb in THz frequency range can be described as the Drude model [Dai (2011); Li (2011)];

$$\varepsilon_B(\omega) = \varepsilon_\infty - \frac{\omega_p^2}{\omega^2 + i\omega\gamma} \quad \ldots\ldots \quad (4.13)$$

where ε_∞ represents the static dielectric constant, γ is the damping constant, plasma frequency $\omega_p = \sqrt{Ne^2/\varepsilon_0 m^*}$ depends on the intrinsic carrier density N, the electric charge e, the effective mass m^* of the free carriers and the free space permittivity ε_0. The plasma frequency ω_p of InSb depends strongly on the temperature T as compare to metals. The intrinsic carrier density N (in m^{-3}) depends on the temperature strongly and obeys the relationship;

$$\boldsymbol{N = 5.76 \times 10^{20} T^{3/2} \exp(-0.13/k_B T)} \quad \text{… …} \quad \textbf{(4.14)}$$

where T is the temperature in kelvin and k_B is the Boltzmann constant. The plasma frequency ω_p depends on temperature T that makes the dielectric function of the semiconductor InSb sensitive to the temperature T, so optical index $n_B(\omega) = \sqrt{\varepsilon_B(\omega)\mu_B}$ also depends on the temperature T and here, permeability $\mu_B = 1$. Herein, we have assumed that the temperature T change from 150 K to 360 K. The variations of optical index n_B at different temperature are shown in the figure 4.19 (c and d). Figures 4.19(c) and 4.19(d) respectively show the real and imaginary part of the optical index. Controlling external temperature provides expect significant variation to tune PBGs.

The electric field distribution for the electromagnetic wave propagation in a graded index layer A, if the refractive index of the graded layer has exponential gradation profile as equation (4.11), can be expressed as;

$$\boldsymbol{E_{AE}(x) = A_E J_0\left(\frac{\xi_E}{\delta}\right) + B_E Y_0\left(\frac{\xi_E}{\delta}\right)} \quad \text{… …} \quad \textbf{(4.15)}$$

where $\xi_E = \frac{\omega}{c} n_{AE}(x)$ is the wave propagation vector for exponential graded layers at normal angle of incidence. Refractive index $n_{AE}(x)$ taken according the exponential graded material defined as above equation (4.11), ω is the angular frequency and c is the velocity of light. Grading profile parameter for exponential graded index layers to be $\delta = \frac{1}{d_1}\ln\left(\frac{n_f}{n_i}\right)$. Therefore, the equation (4.11) can represent as $n(x) = n_i e^{\delta x}$ for the exponential graded index layers (A). A_E and B_E are arbitrary constants for graded layers, J_0 and Y_0 are first and second kind of the 0^{th}-order Bessel function, respectively. Subscript E represents an exponential graded layer. If the refractive index of graded index layer has linear gradation profile as equation (4.12), the electric field distribution for the electromagnetic wave propagation in the layer A can be expressed as;

$$\boldsymbol{E_{AL}(x) = \sqrt{\xi}\,.\left[A_L J_{\frac{1}{4}}\left(\frac{\xi^2}{2\alpha}\right) + B_L Y_{\frac{1}{4}}\left(\frac{\xi^2}{2\alpha}\right)\right]} \quad \text{… …} \quad \textbf{(4.16)}$$

where A_L and B_L are constants for the linear graded index layers, $\xi = \omega.n_{AL}(x)/c$ is the propagation wave vector at normal incidence, ω is the angular frequency and c is the speed of light. Refractive index $n_{AL}(x)$ is defined as above equation (4.12). $J_{1/4}$ and $Y_{1/4}$ are the first and second kind of the $(1/4)^{th}$-order Bessel functions, respectively. Subscript L represents a linear graded layer and $\alpha = (\omega/c).\left(n_f - n_i/d_1\right)$ is the grading profile parameter. The electric field distribution of the electromagnetic waves in a semiconductor InSb layer (B) along x-axis can be expressed as;

$$\boldsymbol{E_S(x) = A_S\, exp(-ik_S x) + B_S\, exp(ik_S x)} \qquad \ldots\ldots \quad \textbf{(4.17)}$$

where A_S and B_S are the constants, $k_S = \frac{\omega}{c}.n_B(\omega)$ is the wave vector at the normal incident and subscript S represents a semiconductor layer.

In order to calculate the reflectance, transmittance, reflection phase shift and dispersion relation of the periodic structure $(AB)^P$, the multilayer interface optics is adopted. Multilayer interface optics can generally be described in terms of amplitudes and phases of light reflected (or transmitted) at material boundaries to produce interference effects. To attain the reflectance (R) and transmittance (T), it is necessary to calculate the reflection (r) and transmission (t) coefficients of the fields in the incident and outgoing media due to partially transmitted and reflected waves generated at each interface in the multilayer. The frequency dependent coefficients A_l and B_l $(l = 1, 2, 3 \ldots\ldots)$ are determined by imposing continuity conditions for both electric field and magnetic field across the interface from one medium to next. This establishes a set of equations for transfer matrix formalism. The set of equations for the periodic structure composed linear graded index material (as layer A) and semiconductor material (as layer B) layer in the air background can be expressed as;

$$\underbrace{\begin{pmatrix} \mathbf{1} & \mathbf{1} \\ \boldsymbol{ik_0} & \boldsymbol{-ik_0} \end{pmatrix}}_{\boldsymbol{M_0}} \begin{pmatrix} \boldsymbol{A_0} \\ \boldsymbol{B_0} \end{pmatrix} = \underbrace{\begin{pmatrix} \sqrt{\xi_0}.J_{\frac{1}{4}}\left(\frac{\xi_0^2}{2\alpha}\right) & \sqrt{\xi_0}.Y_{\frac{1}{4}}\left(\frac{\xi_0^2}{2\alpha}\right) \\ -\left(\frac{\alpha}{2{\xi_0}^{3/2}}.J_{\frac{1}{4}}\left(\frac{\xi_0^2}{2\alpha}\right) + {\xi_0}^{3/2}.J_{\frac{1}{4}}'\left(\frac{\xi_0^2}{2\alpha}\right)\right) & -\left(\frac{\alpha}{2{\xi_0}^{3/2}}.Y_{\frac{1}{4}}\left(\frac{\xi_0^2}{2\alpha}\right) + {\xi_0}^{3/2}.Y_{\frac{1}{4}}'\left(\frac{\xi_0^2}{2\alpha}\right)\right) \end{pmatrix}}_{\boldsymbol{M_i}} \begin{pmatrix} \boldsymbol{A_1} \\ \boldsymbol{B_1} \end{pmatrix}$$

$$\underbrace{\begin{pmatrix} \sqrt{\xi_1}.J_{\frac{1}{4}}\left(\frac{\xi_1^2}{2\alpha}\right) & \sqrt{\xi_1}.Y_{\frac{1}{4}}\left(\frac{\xi_1^2}{2\alpha}\right) \\ -\left(\frac{\alpha}{2{\xi_1}^{3/2}}.J_{\frac{1}{4}}\left(\frac{\xi_1^2}{2\alpha}\right)+{\xi_1}^{3/2}.J_{\frac{1}{4}}'\left(\frac{\xi_1^2}{2\alpha}\right)\right) & -\left(\frac{\alpha}{2{\xi_1}^{3/2}}.Y_{\frac{1}{4}}\left(\frac{\xi_1^2}{2\alpha}\right)+{\xi_1}^{3/2}.Y_{\frac{1}{4}}'\left(\frac{\xi_1^2}{2\alpha}\right)\right) \end{pmatrix}}_{M_f}\begin{pmatrix} A_1 \\ B_1 \end{pmatrix}$$

$$=\underbrace{\begin{pmatrix} 1 & 1 \\ ik_S & -ik_S \end{pmatrix}}_{M_1}\begin{pmatrix} A_2 \\ B_2 \end{pmatrix}$$

$$\underbrace{\begin{pmatrix} e^{-ik_Sd_2} & e^{ik_Sd_2} \\ ik_se^{-ik_Sd_2} & -ik_se^{ik_Sd_2} \end{pmatrix}}_{M_2}\begin{pmatrix} A_2 \\ B_2 \end{pmatrix}$$

$$=\underbrace{\begin{pmatrix} \sqrt{\xi_0}.J_{\frac{1}{4}}\left(\frac{\xi_0^2}{2\alpha}\right) & \sqrt{\xi_0}.Y_{\frac{1}{4}}\left(\frac{\xi_0^2}{2\alpha}\right) \\ -\left(\frac{\alpha}{2{\xi_0}^{3/2}}J_{\frac{1}{4}}\left(\frac{\xi_0^2}{2\alpha}\right)+{\xi_0}^{3/2}J_{\frac{1}{4}}'\left(\frac{\xi_0^2}{2\alpha}\right)\right) & -\left(\frac{\alpha}{2{\xi_0}^{3/2}}Y_{\frac{1}{4}}\left(\frac{\xi_0^2}{2\alpha}\right)+{\xi_0}^{3/2}Y_{\frac{1}{4}}'\left(\frac{\xi_0^2}{2\alpha}\right)\right) \end{pmatrix}}_{M_i}\begin{pmatrix} A_3 \\ B_3 \end{pmatrix}$$

… … so on

where $k_0(=(\omega/c).n_0)$ and $k_S(=(\omega/c).n_B(\omega))$ are the wave vector of the incident (0^{th}) and semiconductor media, respectively and n_0 is the refractive index of air medium. In the case of the graded layers, wave vector at initial boundary is $\xi_0 = \omega.n_i/c$ and at final boundary $\xi_1 = \omega.n_f/c$, where n_i and n_f are the refractive indices at the initial and final boundary of the graded layers, respectively. Matrices M_i and M_f are the 2×2 characteristic matrix at initial and final boundary of the graded index layers, Matrices M_1 and M_2 are the 2×2 characteristic matrix at initial and final boundary of the semiconductor layers.

The expressions of the set of equations across the interface from one medium to the next will be similar for the structures composed exponential graded index material as layer A, but the characteristics matrices (M_i and M_f) at initial and final boundary of the layers A change according to exponential grading profile and electric field distribution expressed as equation (4.14). Thus, for the exponential graded material as layer A, the characteristic matrices M_i and M_f at the initial and final boundary of the exponential graded index layer will be;

$$M_i=\begin{pmatrix} J_0\left(\frac{\xi_i}{\delta}\right) & Y_0\left(\frac{\xi_i}{\delta}\right) \\ \xi_i.J_1\left(\frac{\xi_i}{\delta}\right) & \xi_i.Y_1\left(\frac{\xi_i}{\delta}\right) \end{pmatrix} \text{ and } M_f=\begin{pmatrix} J_0\left(\frac{\xi_f}{\delta}\right) & Y_0\left(\frac{\xi_f}{\delta}\right) \\ \xi_f.J_1\left(\frac{\xi_f}{\delta}\right) & \xi_f.Y_1\left(\frac{\xi_f}{\delta}\right) \end{pmatrix},$$

where wave vector at initial boundary is $\xi_i = \omega.n_i/c$ and at final boundary is $\xi_f = \omega.n_f/c$, where n_i and n_f are the refractive index at the initial and final boundary of the

exponential graded index layer, respectively. $J_{0(1)}$ and $Y_{0(1)}$ are first and second kind of the 0^{th}-order (1^{st}-order) Bessel function, respectively.

To investigate the propagation properties of the electromagnetic wave in the periodic structure $(AB)^P$, where P is the number of periods. We embrace the transfer matrix method to calculate the reflectance and band gap spectra. After applying the transfer matrix approach on the considered structures, the electromagnetic wave propagates through the whole structures can be expressed by multiplying the characteristic matrices of the constituent layers as;

$$\begin{pmatrix} A_0 \\ B_0 \end{pmatrix} = M_0^{-1}.(M_G.M_S)^P.M_0 \begin{pmatrix} A_{2n+1} \\ 0 \end{pmatrix} \quad \ldots\ldots \quad \textbf{(4.18)}$$

where P is the number of periods, A_0, B_0 and A_{2n+1} are the constant for incident (0^{th}) media and outgoing $(2n+1)^{th}$ media, respectively. Matrices $M_{G,}$ M_S and M_0 are the 2x2 characteristics matrix for graded index layer, semiconductor layer and air media, respectively. Subscript G and S represent a graded index and semiconductor layers, respectively. The characteristics matrices are $M_G = M_i.{M_f}^{-1}$ and $M_S = M_1.{M_2}^{-1}$. Matrices $M_i$and M_f are the 2x2 characteristics matrices at initial and final refractive index boundary of the graded layers, $M_1$and M_2 are the 2x2 characteristics matrices at initial and final boundary of the semiconductor layers as given in the set of equations for the interface from one medium to the next.

If the electric field is known at beginning of the system, the field at the end of the system can be derived from a simple matrix operation as shown in the above sets of equations. A stack of layers can then be represented as a complete system matrix, which is the product of the individual matrices corresponding to each intermediate layer within the considered structures. In this way, it can be directly obtained the relations between reflection (r) and transmission (t) coefficients of the fields in the incident and outgoing media. Therefore, reflectance (R) and transmittance (T) of the structures are determined using the following relations;

$$R = |r|^2 = \left|\frac{B_0}{A_0}\right|^2 \; and \quad T = |t|^2 = \left|\frac{A_{2n+1}}{A_0}\right|^2 \quad \ldots\ldots \quad \textbf{(4.19)}$$

The reflection phase shift (Φ) of the optical waves from the PC structures is also of particular interest. The reflection phase shift relation with reflection coefficient is obtained as [Yariv (2007)];

$$r = |r|.e^{-i\Phi} \quad \ldots\ldots \quad (4.20)$$

By calculating the phase shifts in the reflected light at different temperatures, we are able to figure out the phase change in PBGs relative to the temperatures. The phase shift exhibits a strong dispersion as a function of the frequency. The dispersion is an equation relating the Bloch wave number K and the angular frequency ω, and that has been derived for infinite periodic structure using the transfer matrix method as;

$$K(\beta, \omega) = \frac{1}{d}.cos^{-1}\left\{\frac{1}{2}(M_{11} + M_{22})\right\} \quad \ldots\ldots \quad (4.21)$$

where d is the total thickness of a period, M_{11} and M_{22} is the elements of the 2x2 optical transfer matrix $M_{i,j}(i, j = 1, 2)$. The optical transfer matrix is $M_{i,j} = M_G.M_S$ for the structure composed with graded index layer A and semiconductor layer B.

The dispersion relation exhibits multiple spectral bands classified into two regimes. First, where $|(M_{11} + M_{22})/2| \leq 1$ corresponds to real K implies to propagating Bloch waves. Second, spectral bands within which K is complex correspond to evanescent waves that are rapidly attenuated. Defined by the condition $|(M_{11} + M_{22})/2| > 1$, these bands correspond to the stop bands of the systems known as photonic band-gaps [Yeh (1988); Yariv (2007)].

4.3.2 Numerical results and discussion

In this section, we have demonstrated the effect of temperature, lattice parameter, grading parameter and damping loss on the PBGs in the periodic structure $(AB)^P$. In order to obtain the PBG in terahertz frequency region, we choose semiconductor InSb for the medium B, expression of permittivity $\varepsilon_B(\omega)$ is as equation (4.13) and permeability $\mu_B = 1$. The linear and exponential graded index materials are assumed for the medium A and the refractive index n_A for exponential and linear graded index is given as the equation (4.11) and (4.12), respectively. Our results observation has been carried out in the following parts.

4.3.2.1 Effect of temperature on the photonic band gaps

First, the reflection spectra of the structure $(AB)^{10}$ at different temperature are shown in the figures 4.20(a - e). Here, the structural parameters assume as; $d_A = 5\ \mu m$, $d_B = 1\ \mu m$, $n_i = 1.5$, $n_f = 4.5$, $\gamma = 0$, $\varepsilon_\infty = 15.68$, $m^* = 0.015m_e$, $m_e = 9 \times 10^{-31}$ kg. To simplify our calculation, we assume that light incident through the air medium and the losses of the constituted material are neglected. It can clearly see in the

figure 4.20 that the edges of PBG shift upward in frequency with increasing the temperature. The shifting of the edges of higher order band gap is very slow. From all these figures, it is clearly visible that the band gaps of the structure with exponential graded index material are wider as compare to the band gaps of the structure with linear graded index material.

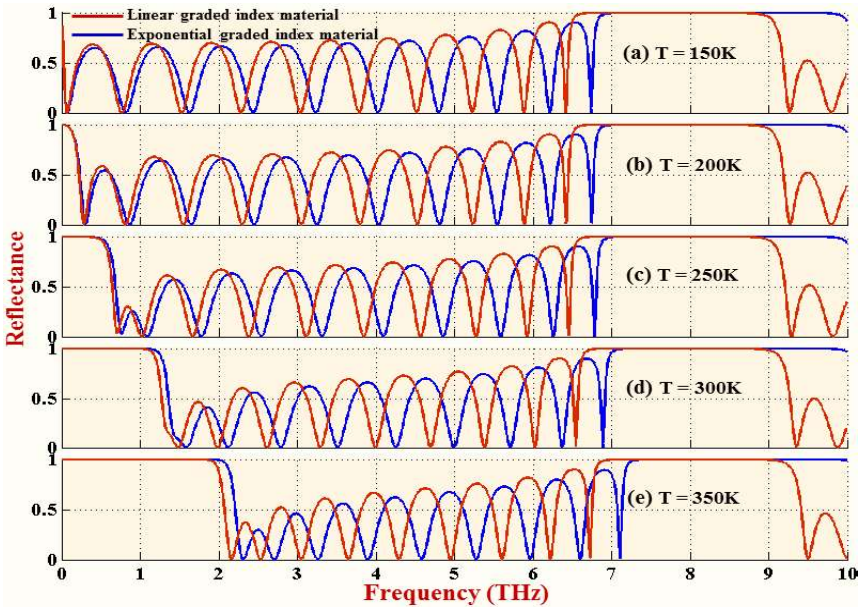

Figure 4.20 The reflectance as a function of frequency with varying temperature and layer thicknesses d_1 = 5 μm and d_2 = 1 μm for the 1-D PC structure $(AB)^{10}$ with linear and exponential graded index materials.

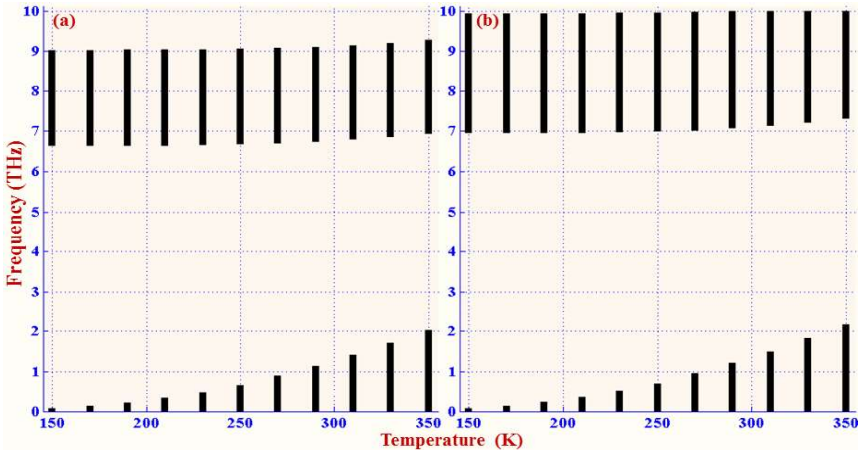

Figure 4.21 The distribution of the photonic band gaps (black region) as a function of the temperature for the PC structure $(AB)^{10}$ with (a) linear and (b) exponential graded index materials. Layer thicknesses are d_1 = 5 μm and d_2 = 1 μm.

In order to discuss the variation of PBGs with temperature, we have calculated the regions for forbidden frequencies (stop bands), where $|(M_{11} + M_{22})/2| > 1$, as a function of the temperature and depicted in the figures 4.21(a and b) for the structures

with linear and exponential graded index materials, respectively. These figures show the distribution of the forbidden (black region) and allowed (white region) frequency regions as a function of the temperature up to 350 K. As expected, the forbidden band gaps observed at zero transmission intensity range and that increase with temperature.

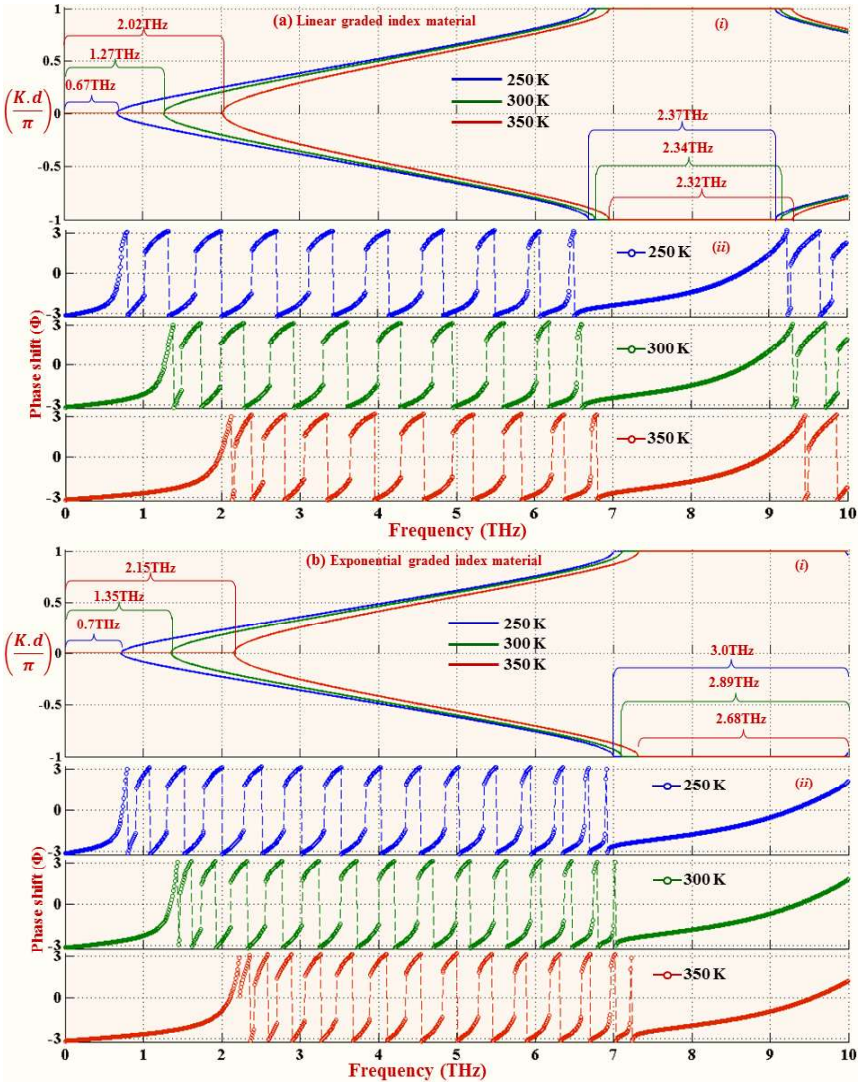

Figure 4.22 Panels (i) dispersion spectra and panels (ii) reflection phase shifts for the periodic structure with (a) linear and (b) exponential graded index materials at different temperatures.

Moreover, we would like to extend the study on the dispersion curves and reflection phase shift associated with the wider PBGs. For different temperature, dispersion curves are calculated from equation (4.21) for the unbounded periodic structures and shown in the panel (i) of figures 4.22(a and b) as a function of the reduced Bloch wave vector kd/π, and related reflection phase shifts are likewise illustrated in the panel (ii) for the structures with linear and exponential graded index materials, respectively. Also as seen

here, the bandwidth of forbidden bands increases and shifted towards higher frequency region, when temperature increases. Moreover, we watch in the panels (ii) of figures 4.22(a and b), and observe that the reflection phase shifts varies from close to -π at one band edge to approximate +π at another band edge of the stop bands. The edges of reflection phase shifts also shift with temperature due to change of the position of band edges of forbidden band gaps. Reflection phase shift changes precipitously in the pass bands region, while it changes gradually in the forbidden band gaps region. Reflection phase shifts can also be changed with arrangement of layers in unit cells of the structure, incident angles and polarizations [Dai (2010); Lui (2015)]. Herein, reflection phase shifts are also different for the structures with linear and exponential graded index material layers, while initial and final refractive index are same for both linear and exponential graded index layers.

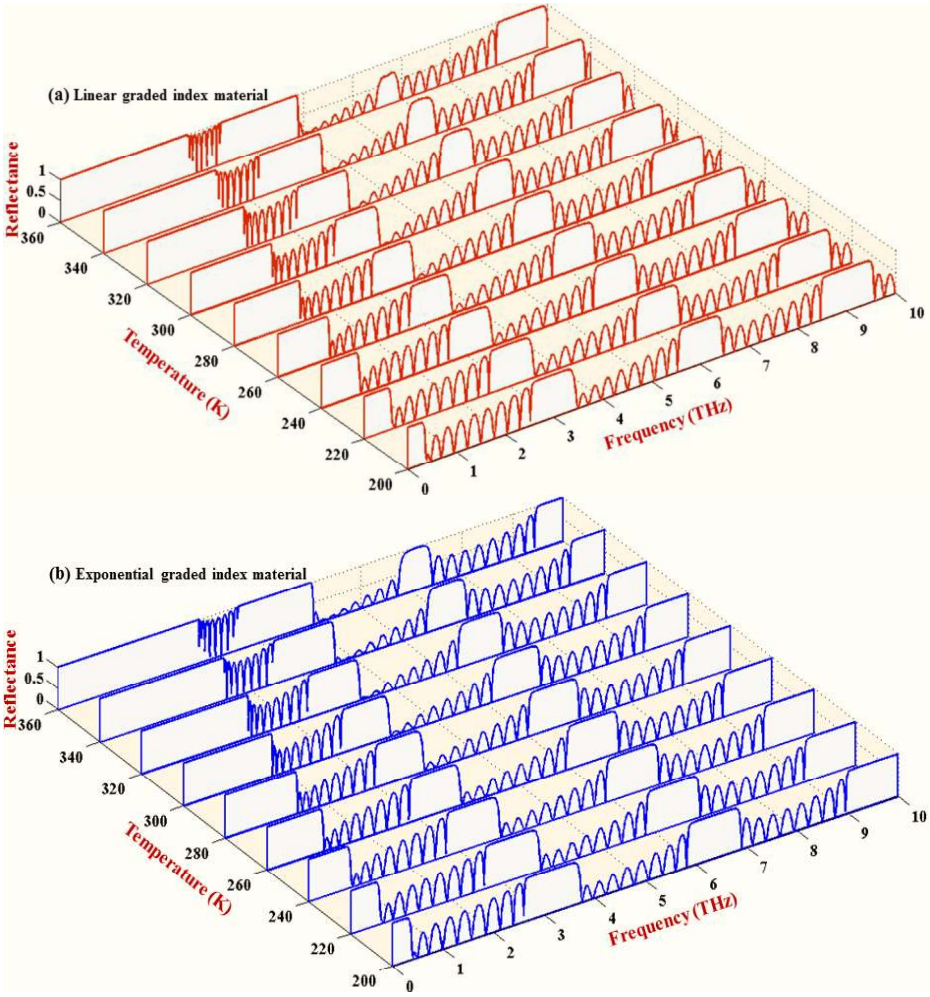

Figure 4.23 Reflection spectra for the structure $(AB)^{10}$ with (a) linear and (b) exponential graded index materials as a function of frequency with the varying temperature and layers thickness $d_1 = 10$ μm and $d_2 = 5$ μm.

Due to the important of the influence of temperature on the PBGs, we would like to extend the study on the reflectance associated with the PBGs in the structure with exponential and linear graded index materials. Figures 4.23(a) and 4.23(b) give the dependence of the reflection coefficient on the frequency and temperature for the structure with exponential and linear graded index materials, respectively. It is clearly demonstrated that there exist four photonic bands at layers thickness d_1 = 10 μm and d_2 = 5 μm, where electromagnetic wave cannot be transmitted. With the temperature increasing, the bandwidth of lower photonic bands increases and the bandwidth of higher photonic bands decreases. The edges of PBGs shifted upward in frequency with increasing temperature. The PBG properties are basically affected by the contrast of refractive index of the constituted media. With increasing the temperature, the average volume of refractive index in semiconductor layer increases so the refractive index contrast of the system enhanced and hence influence of the Bragg stack become more effectively.

For better understanding the effect of temperature on electromagnetic wave propagation in the considered structures, we have calculated the spatial distribution of the square magnitude of the electric field at selected frequencies impinging under different reflection conditions at temperatures 200 K, 250 K, 300 K and 350 K in the structures with graded index and semiconductor materials. The electric field is denoted by the E(x). For the sake of clarity, we have chosen the thickness of layers as d_1 = 12 μm and d_2 = 5 μm for better understanding of the effect of electric field. Figures 4.24(a) and 4.24(b) show the distribution of electric field in the structures with linear and exponential graded index materials, respectively. In the insets of the figures 4.24(a) and 4.24(b), we have shown the reflectance spectra for the relative structures. Results show the reflection spectra at different temperature for the structures with linear and exponential graded index materials. It can clearly see that at frequencies 8.59 THz and 9.15 THz, reflection coefficient change with temperature. We have focused the electric fields corresponding to the gap-edge frequencies 8.59 THz and 9.15 THz for structures with linear and exponential graded index materials, respectively. In figure 4.24, we have calculated the square magnitude of electric field inside the structures at frequencies 5.89 THz and 9.15 THz for temperature 200 K, 250 K 300 K and 350 K. The electric field intensities change due to change the values reflection coefficient with temperature. The electric field distributions in the graded layers for different grading profiles are

different, although the initial and final refractive indices of graded index layers are same. The electric field intensities decrease as increasing the propagating depth of graded layers with linearly and exponentially increasing refractive index as illustrated in the panels (a) and (b) of the figure 4.24, respectively. The electric field intensities in graded layers for exponential gradation profiles are larger than electric field intensities for linear gradation case. The electric field corresponding to the frequencies 8.59 THz and 9.15 THz concentrate their energy in the structures for 0% reflection at temperature 250 K. With increasing the reflection coefficients, the electric field intensity in the structure decreases with depth. The characteristics of the electric field distribution in the structures lead to the change of reflection spectra of the structures.

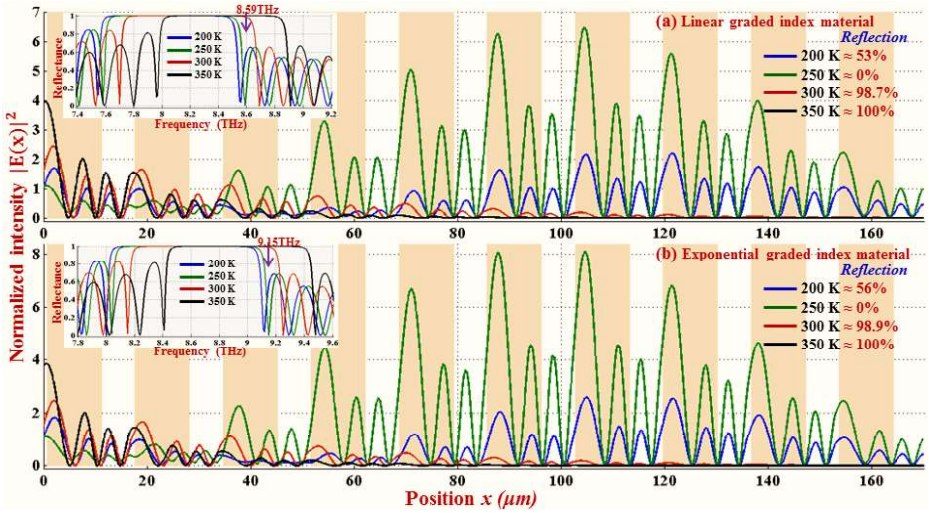

Figure 4.24 The distributions of the electric field intensity in the system $(AB)^{10}$ with (a) linear and (b) exponential graded index materials at frequencies 8.59 THz and 9.15 THz, respectively with four selected temperature 200 K, 250 K, 300 K and 350 K, and layer thickness $d_1 = 12$ μm and $d_2 = 5$ μm. Reflection spectra around the frequency 8.59 THz and 9.15 Thz are shown in insets of the panels (a) and (b), respectively.

4.3.2.2 Effect of layer thickness on the photonic band gaps

To disclose the dependence of PBGs on the layers thickness, we have shown the reflection spectra of the structure $(AB)^P$ at different thickness of constituents in the figures 4.25(a - e), here temperature T = 300 K and P = 10. It is clear that the number of photonic bands increases with layer thickness and their bandwidths become narrow as increasing the bands. Formation of photonic bands are approximate similar for structures with linear and exponential graded index materials but their bandwidth for the structure with exponential graded index material are slightly larger as compare to linear graded index material. Band gap regions for the structure with exponential graded index

material exist at higher frequency regions as compare to the band gap regions for the structure with linear graded index material. Thickness of semiconductor layers is more sensitive for the generation of PBGs.

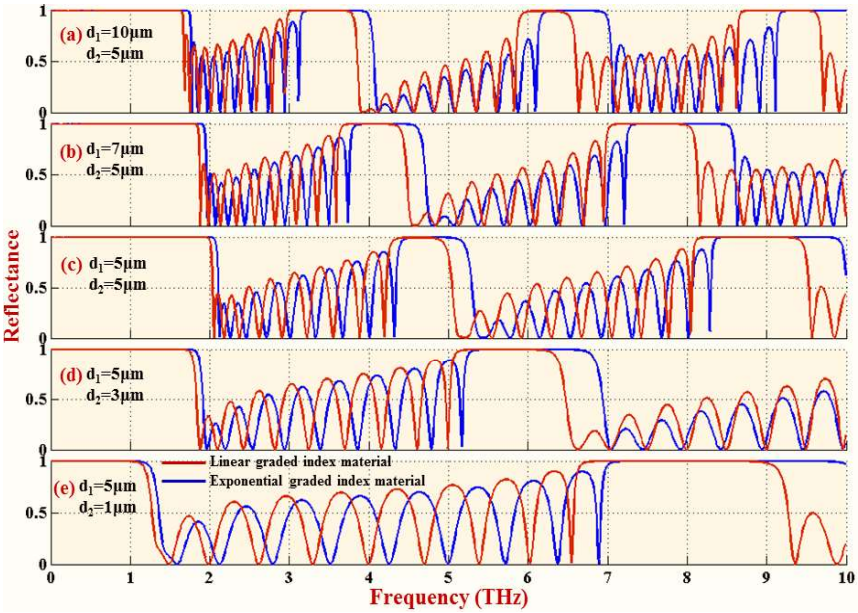

Figure 4.25 Reflection spectra as a function of frequency with varying layer thickness d_1 and d_2 for the structure $(AB)^{10}$ with linear and exponential graded index materials at temperature T = 300 K.

Now, we examine the confinement effects arising from competition between the structures induced by changing the thickness of layers and magnitude of the total stop bandwidths in the PBG spectra. To do that, we have calculated the regions for forbidden frequencies as a function of the layers thickness and depicted in the figures 4.26 and 4.27. In the figure 4.26, the thickness of semiconductor layer assume as d_B = 1 μm to study the dependence of the photonic band gaps on the thickness ratio (d_A/d_B). The distributions of the forbidden (black region) and allowed (white region) frequencies as a function of the thickness ratio (d_A/d_B) for the structures with linear and exponential graded index materials are shown in the figures 4.26(a) and 4.26(b), respectively. It is clearly seen that more and more photonic band gap appear as the increase of thickness ratio (d_A/d_B) and their bandwidth become narrower and narrower as increasing the number of forbidden bands. Moreover, we observe number of forbidden bands are approximate same for the structures with linear and exponential graded index materials but their band regions and bandwidths are different. The bandwidth of PBGs in the structures with exponential graded index material is high as compare to the structures with linear graded index material.

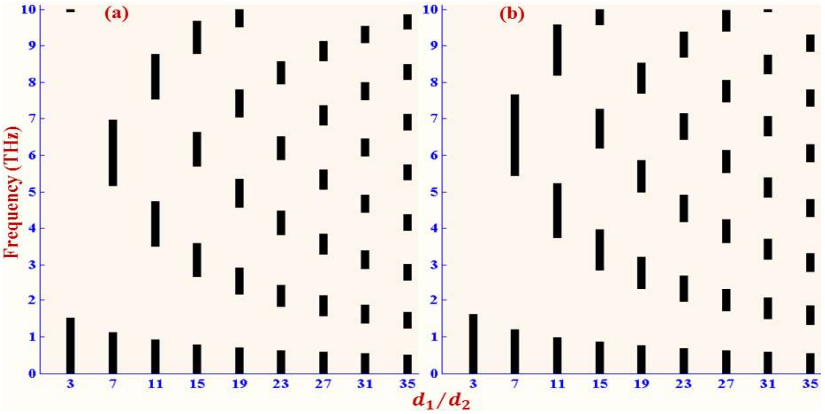

Figure 4.26 The distribution of the photonic band gaps (black region) as a function of the thickness ratio (d_1/d_2) for the periodic structure $(AB)^P$ with (a) linear and (b) exponential graded index materials, where $d_2 = 1$ μm and T = 300 K.

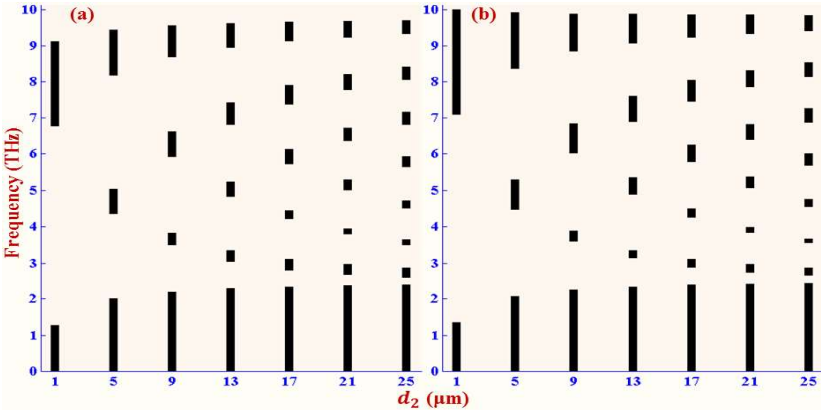

Figure 4.27 The distribution of the photonic band gaps (black region) as a function of the thickness d_2 for the periodic structure $(AB)^P$ with (a) linear and (b) exponential graded index materials, where $d_1 = 5$ μm and T = 300 K.

The distribution of the forbidden (black region) and allowed (white region) frequencies as a function of the layer thickness d_B for the structures with linear and exponential graded index materials are shown in the figures 4.27(a) and 4.27(b), respectively while thickness of graded index layer is assume as $d_A = 5$ μm. As expected, the number of forbidden bands also increases with semiconductor layer thickness d_B and their bandwidth becomes narrower and narrower as increasing the number of forbidden bands. But semiconductor layer thicknesses are more effective on to form of new PBGs. Similar as above, the bandwidth of PBGs in the structures with exponential graded index material is large as compare to structures with linear graded index material.

4.3.2.3 Effect of grading parameter on the photonic band gaps

To investigate the effects of grading parameters on the PBGs, we have investigated the reflectance and band gap spectra at different grading parameters under

normal incidence. The reflection spectra for the structure with exponential and linear graded index materials at different values of n_f are shown in the figures 4.28(a) and 4.28(b), respectively and here structural parameters are d_1 = 10 μm, d_2 = 5 μm and T = 300 K. When the values of n_f increases, lower and upper band-edges shift to lower frequency and new band gap generates at higher frequency region. Bandwidth of lower band gaps decreases while bandwidth of higher band gaps increases with increasing the values of n_f.

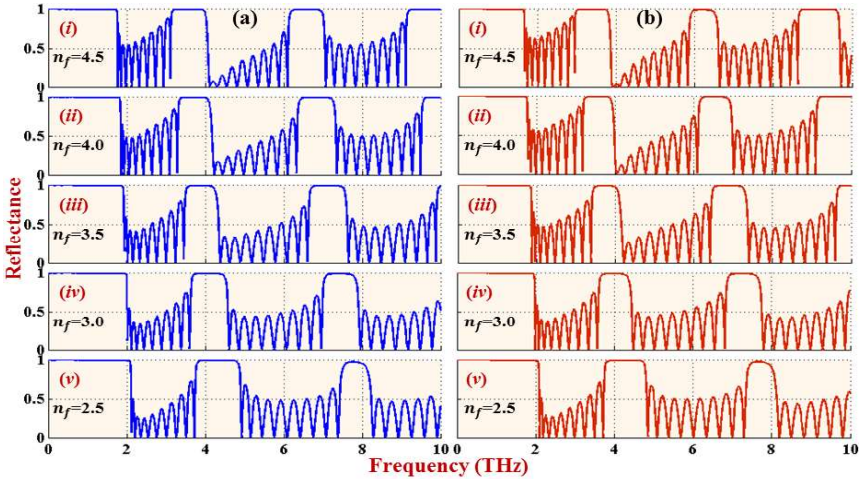

Figure 4.28 Reflection spectra at different values of $\boldsymbol{n_f}$ for the structure $(AB)^{10}$ with (a) linear and (b) exponential graded index materials at temperature T = 300 K, and layer thickness d_1 = 10 μm and d_2 = 5 μm, and refractive index $\boldsymbol{n_i}$ = 1.5.

To take a close look of the dependence of PBGs on the grading parameters, we now demonstrate the forbidden band gaps as a function of n_f and n_i in the figures 4.29 and 4.30, respectively. The black regions show the forbidden frequency regions. First, we have calculated the forbidden frequency regions as a function of refractive index n_f and depicted in the figures 4.29(a) and 4.29(b), respectively for the structure with linear and exponential graded index materials. Here, the structural parameters assumed as; d_1 = 5 μm, d_2 = 1 μm, T = 300 K and n_i = 1.5. Now, we have considered a fixed refractive index n_f = 4.5 and calculated the stop band frequency regions as a function of the refractive index n_i. Figures 4.30(a) and 4.30(b) are showing the PBG spectra as a function of the refractive index n_i for the structures with linear and exponential graded index materials, respectively. In both cases, the bandwidth of first and second PBGs change with the value of refractive indices n_i and n_f. The PBG properties are basically modulated by the contrast of optical index of the constituted media. With decreasing the refractive index n_f or increasing the refractive index n_i, the rate of change of refractive

index of the constituted media decreases and hence the Bragg affect become less effective. Therefore, the bandwidth and frequency region of forbidden ban gaps are modulated by changing the gradation parameters.

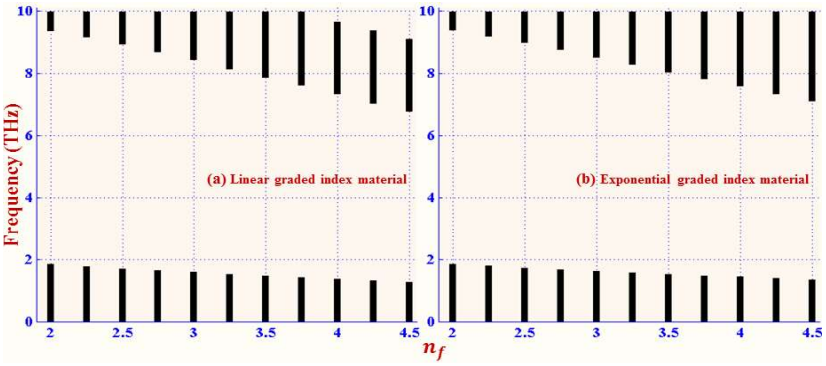

Figure 4.29 The distribution of forbidden band gaps (black region) as a function of refractive index $\boldsymbol{n_f}$ of the graded layer for the structure $(AB)^P$ with (a) linear and (b) exponential graded index materials, here d_1 = 5 μm, d_2 = 1 μm, $\boldsymbol{n_i}$ = 1.5 and T = 300 K.

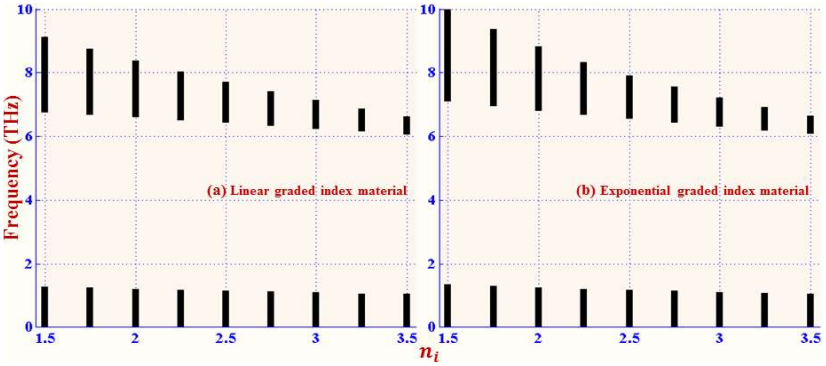

Figure 4.30 The distribution of forbidden band gaps (black region) as a function of refractive index $\boldsymbol{n_i}$ of the graded layer for the structure $(AB)^P$ with (a) linear and (b) exponential graded index materials, here d_1 = 5 μm, d_2 = 1 μm, $\boldsymbol{n_f}$ = 4.5 and T = 300 K.

In above demonstrations, we have neglected the damping constant (γ) in the semiconductor material InSb. In practice, the loss in the semiconductor material is invertible. When losses are involved, the properties of PBGs will be slightly degraded. In figure 4.31, we have calculated the reflectance at different values of damping factor (γ) for the structures with linear and exponential graded index materials. We can clearly see that the loss only decrease the transmittance intensity of the lower-order photonic band gap (Gap I) while higher-order photonic band gaps are invariant on the loss of semiconductor. Figure 4.31 shows the reflectance intensity of the Gap I which slightly increases to ideal value due to the loss of semiconductor material i.e. damping constant γ. But the higher-order PBGs (Gap II and III) are invariant on the damping factor γ up to $2\pi\times0.002$ THz. When the values of damping constant $\gamma > 2\pi\times0.002$ THz, reflectance

intensities of the higher-order PBGs are also change with damping constant because semiconductor material layers in the structures are absorbing more incident light.

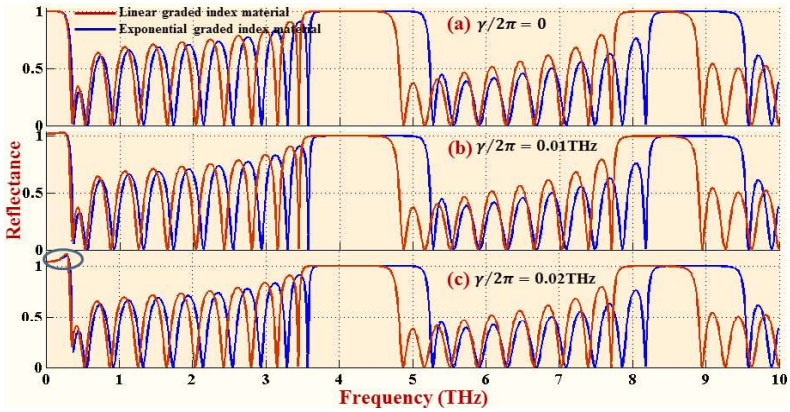

Figure 4.31 Reflection spectra at different values of damping factor γ for the structure $(AB)^{10}$ with linear and exponential graded index materials, here temperature T = 200 K, refractive index $\boldsymbol{n_i}$ = 1.5 and $\boldsymbol{n_f}$ = 4.5, layer thickness d_1 = 8 μm and d_2 = 3 μm.

4.4 Conclusion

In this chapter, the PBG properties of the 1-D PC structures composed of exponential graded index material and dispersive materials (metamaterials and semiconductor) have been presented. In the first case, the PC structures are considered with three different kind metamaterials. Initially, considered as a negative index material that has simultaneously negative permittivity and permeability and in other cases, metamaterials are considered as a single negative material in which only one of the material parameters has a negative value. These single negative materials include the epsilon-negative media with negative permittivity but positive permeability, and the mu-negative media with negative permeability but positive permittivity. In the case of the structure with the stack of exponential graded index material and negative index material, the number and bandwidth of PBGs increase with increasing the negative index material layer thickness while the thickness of graded layer only affects to the bandwidth. The bandwidth of PBG can also be tuned by grading parameters. In addition, the Omni-directional bands also exist in such structures. Omni-directional bands increase with the increase of the negative index layer thickness, but one has broader bandwidth and others become narrow and narrow. The bandwidth and band range can also be controlled by graded layers thickness and grading parameters. In the case of the periodic structure with exponential graded index and epsilon-negative (ε<1, μ=1) materials, two PBGs obtain at higher values of layer thickness. One of the bands is

in lower frequency region and the other in higher frequency region from the central frequency. Their bandwidth increases with increasing the layers thickness. Thickness of the graded layers has very small effect on the first band gap but second band gap decreases and shifted with deceasing the graded layers thickness. The bandwidth and generation of second band can also be controlled by grading parameters. Moreover, two omnidirectional bands also exist in this structure at higher layer thickness ratio. One of the omnidirectional bands is in lower frequency region and the other at higher frequency region from the central frequency. Their bandwidth increases with thickness of layers. In the case of the periodic structure with exponential graded index and mu-negative (ε=1, μ<1) materials, single broader PBG is obtained. Their bandwidth gradually increases with increasing the thickness of mu-negative material layers while bandwidth slightly increases with decreasing the graded layer thickness. For such type of structures, the grading parameters have no especial affect to control the bandwidth of PBG. Here, the bandwidth of PBG only can be modulated by layers thickness. A single wide omnidirectional band is also observed for this structure. The bandwidth of OBG can be slightly modulated with the thickness of constituted layers. Thus, the photonic and Omni-directional band gaps with desire band region and bandwidth can be achieved by selecting the related parameters of the structures with graded materials and different types of meta-materials. Accordingly, our proposed structures can be used to design various optical filters, mirrors and sensors etc.

In the second case, we been demonstrated the effect of semiconductor on the PBGs in 1-D GPC structures constituted with semiconductor in THz region. The number of PBGs increases with layers thickness and temperature. The frequency range and bandwidth of PBGs can be modulated by controlling the temperature. The frequency range and bandwidth of the PBGs can also be tuned with the grading parameters and profiles. Temperature, gradation profiles and parameters have a substantial influence on the band structure, phase and electric field distribution in the proposed structure. We expect to achieve desired and tunable PBGs by selecting appropriate structural parameters and temperature. Accordingly, considered structures can be utilized to design tunable filters, reflectors, sensors, and other optical devices in THz range.

★★★★★★